Pak.j.stat.oper.res. Vol.21 No. 3 2025 pp 403-427 DOI: https://doi.org/10.18187/pjsor.v21i3.4750

Pakistan Journal of Statistics and Operation Research

A Flexible Discrete Rayleigh-G Family for Engineering and Reliability Modeling: Properties, Characterizations, Bayesian and Non-Bayesian Inference

Mohamed Ibrahim[1,*], G.G. Hamedani[2], M. I. Khan[3], Ahmad M. AboAlkhair[1], Nazar Ali Ahmed[1] and Aya Shehata Mahmoud[4]

* Corresponding Author

[1]Department of Quantitative Methods, School of Business, King Faisal University, Al Ahsa 31982, Saudi Arabia; M.I: miahmed@kfu.edu.sa; A.M.A: aaboalkhair@kfu.edu.sa & nahmed@kfu.edu.sa
[2]Department of Mathematical and Statistical Sciences, Marquette University, USA; gholamhoss.hamedani@marquette.edu
[3] Department of Mathematics, Faculty of Science, Islamic University of Madinah, Madinah 42351, Saudi Arabia; khanizhar@iu.edu.sa
[4]Department of Statistics, Mathematics and Insurance, Faculty of Commerce, Benha University, Benha 13518, Egypt; aya.shehata@fcom.bu.edu.eg

Abstract

A novel flexible probability tool for modeling extreme and zero-inflated count data with various hazard rate shapes is introduced in this work. Numerous pertinent statistical and mathematical features are developed and examined. Some important mathematical features are obtained, including, ordinary moments, central moment, dispersion index, L-moments, cumulant generating function and moment generating function. A specific example is investigated numerically and visually examined. The new class of hazard rate function offers a broad range of flexibility, including "monotonically decreasing," "upside down," "monotonically increasing," "constant," "decreasing-constant," and "decreasing-constant-increasing (U-hazard rate function)". Furthermore, the new mass function accommodates many useful forms in the field of modeling, including the "right skewed with one peak", "right skewed with two peaks (right skewed and bimodal)", "symmetric mass function" "left skewed with one peak". The conditional expectation of a certain function of the random variable as well as the hazard function are used to provide relevant characterization results. For the estimation process, evaluating and comparing inferential effectiveness, Bayesian and non-Bayesian estimation approaches are taken into consideration. We propose and explain the Bayesian estimation method for the squared error loss function. For comparing non-Bayesian versus Bayesian estimates, Markov chain Monte Carlo simulation experiments are carried out using the Metropolis Hastings algorithm and the Gibbs sampler. The Bayesian and non-Bayesian approaches are compared using four real-life applications of count data sets. By using four additional real count data applications, the significance and adaptability of the new discrete class are demonstrated.

Keywords: Bayesian Estimation; Discretization; Metropolis-Hastings; Markov Chain Monte Carlo; Maximum Likelihood; Cramér-von-Mises; Squared Error Loss Function; Zero-inflated Count Data

Key Words: Bayesian Estimation; Count Data; Characterizations; Discrete Family; Dispersion Index; Engineering Applications.

1.Introduction and genesis

In recent years, discretization of known continuous probability distributions has received a great deal of attention. The discrete Rayleigh G family of distributions, a novel discrete counterpart based on the continuous Rayleigh distribution, is presented, and studied in this work. Moments, the cumulant generating function, the moment generating function, the probability generating function, the central moment, and the dispersion index (DisIx) are among the pertinent mathematical features that are calculated and analyzed. It is described how a particular variation of the new family relates to the well-known Weibull model. There are a few traditional (non-Bayesian) estimation techniques that are discussed and taken into consideration, including the Cramér-von-Mises estimation (CVME), the ordinary least squared estimation (OLSE), the maximum likelihood estimation (MLE), and the weighted least squared estimation

(WLSE). Since there are no conventional ways to acquire the conditional posteriors of the parameters, it is advised to take samples from the joint posterior of the parameters using a hybrid Markov chain Monte Carlo method.

Additionally, the squared error loss function Bayesian estimating method is described. To compare non-Bayesian versus Bayesian estimates, Markov chain Monte Carlo simulations are used. Both the Gibbs sampler and the Metropolis Hastings algorithms are used. Four genuine data sets serve as illustrations of the adaptability and significance of the new family. A better match is offered by the new family than by the sixteen rival families. Future research and consideration might be given to a variety of particular member distributions. One may take into account the bivariate and multivariate expansions of this new family in future study. The Rayleigh model is a continuous probability distribution for nonnegative-valued random variables (RVs) that is used in probability and statistics literature. It is consistent with the chi-square distribution with two degrees of freedom up to rescaling. When the total size of a vector is correlated with its directional components, a Rayleigh distribution is commonly seen relevant. The Rayleigh distribution may naturally appear, for illustration, when the two-dimensional analysis of wind velocity is performed. The total wind speed (vector magnitude) will be characterized by a Rayleigh model if each component has zero mean, equal variance, and is normally distributed. The case of random complex numbers with real and imaginary components that are independently and identically distributed as Gaussian with equal variance and zero mean provides a second illustration of the distribution. In that case, the complex number's absolute value has a Rayleigh distribution.

A RV X is said to have Rayleigh model if its cumulative distribution function (CDF) is given by

$$F_{\alpha}(x) = 1 - exp[-(\alpha x)^2]\,|_{(x\geq 0 \text{ and } \alpha>0)}.$$

The generated Rayleigh G (GRG) family's CDF may then be calculated as

$$F_{\alpha,\sigma,\underline{\boldsymbol{\Psi}}}(x) = 1 - exp\left\{-\left[\alpha \boldsymbol{H}_{\sigma,\underline{\boldsymbol{\Psi}}}(x)\right]^2\right\}|_{(x\in R,\sigma>0)}.$$

The function $\boldsymbol{H}_{\sigma,\underline{\boldsymbol{\Psi}}}(\cdot)$ refers to the generated odd ration function, where

$$\boldsymbol{H}_{\sigma,\underline{\boldsymbol{\Psi}}}(\cdot) = \frac{G^{\sigma}_{\underline{\boldsymbol{\Psi}}}(\cdot)}{1 - G^{\sigma}_{\underline{\boldsymbol{\Psi}}}(\cdot)},$$

and $G^{\sigma}_{\underline{\boldsymbol{\Psi}}}(\cdot)$ refers to the CDF of the exponentiated base line model. Let

$$\alpha^2 = -\log(\pi),$$

then, the CDF of the discrete generated Rayleigh G family (DGR-G) can be expressed as

$$F_{\pi,\underline{\boldsymbol{\Psi}}}(x) = 1 - \pi^{\boldsymbol{H}^2_{\sigma,\underline{\boldsymbol{\Psi}}}(x+1)}\;|_{(\pi\in(0,1) \text{ and } x\in \boldsymbol{\mathcal{N}}^{\bullet}=\boldsymbol{\mathcal{N}}\cup\{0\})}. \tag{1}$$

It is possible to write the corresponding reliability function (RF) as

$$S_{\pi,\sigma,\underline{\boldsymbol{\Psi}}}(x) = \pi^{\boldsymbol{H}^2_{\sigma,\underline{\boldsymbol{\Psi}}}(x+1)}\;|_{(\pi\in(0,1) \text{ and } x\in \boldsymbol{\mathcal{N}}^{\bullet})}. \tag{2}$$

The probability mass function (PMF) of the discrete counterpart of the DGR-G family corresponding to (2) may be written, thanks to Kemp (2004), as

$$f_{\pi,\sigma,\underline{\boldsymbol{\Psi}}}(x) = S_{\alpha,\sigma,\underline{\boldsymbol{\Psi}}}(x-1) - S_{\pi,,\sigma,\underline{\boldsymbol{\Psi}}}(x).$$

Therefore, the PMF can be expressed as

$$f_{\pi,\sigma,\underline{\boldsymbol{\Psi}}}(x) = \pi^{\boldsymbol{H}^2_{\sigma,\underline{\boldsymbol{\Psi}}}(x)} - \pi^{\boldsymbol{H}^2_{\sigma,\underline{\boldsymbol{\Psi}}}(x+1)}\;|_{(\pi\in(0,1) \text{ and } x\in \boldsymbol{\mathcal{N}}^{\bullet})}, \tag{3}$$

where $H_{\sigma,\underline{\boldsymbol{\Psi}}}(x)$ refers to function of the generated odd ratio of any discrete non-negative random variable (NNRV) X. The DGR-G family's hazard rate function (HRF) may be expressed as $h_{\pi,\sigma,\underline{\boldsymbol{\Psi}}}(x) = f_{\pi,\sigma,\underline{\boldsymbol{\Psi}}}(x)/S_{\pi,\sigma,\underline{\boldsymbol{\Psi}}}(x-1)$, then

$$h_{\pi,\sigma,\underline{\boldsymbol{\Psi}}}(x) = 1 - \pi^{\boldsymbol{H}^2_{\sigma,\underline{\boldsymbol{\Psi}}}(x+1) - \boldsymbol{H}^2_{\sigma,\underline{\boldsymbol{\Psi}}}(x)}. \tag{4}$$

In the statistical literature, many discrete versions of the continuous distributions have been proposed and studied such as a generalization of the Poisson distribution by Consul et al. (1973), the discrete Weibull distribution (DW) by Nakagawa and Osaki (1975), the discrete Rayleigh distribution (DR) by Roy (2004), discrete half-normal distribution by Kemp (2008), discrete Pareto distribution (DPa) by Krishna and Pundir (2009), a novel discrete geometric distribution (DGc) by Gomez-Déniz (2010), the discrete inverse-Weibull distribution (DIW) by Jazi et al. (2010), the discrete Lindley distribution (DLi) by Gommez-Déniz and Calderin-Ojeda (2011), the discrete generalized exponentiated type II distribution (DGE-II) by Nekoukhou et al. (2013), the discrete inverse Rayleigh distribution (DR) by Hussain and Ahmad (2014), the exponentiated discrete Weibull distribution (EDW) by Nekoukhou and Bidram (2015), the discrete Lomax distribution (DLx) by Para and Jan (2016), discrete log-logistic model (DLL) by Para and Jan (2016), the discrete Lindley type II distribution (DLi-II) by Hussain et al. (2016), the discrete Burr type XII distribution (DBXII) by Para and Jan (2016), the exponentiated discrete Lindley distribution (EDLi) by El-Morshedy et al. (2020), Discrete Burr-Hatke model with some properties, different estimation methods and regression

modeling by El-Morshedy et al. (2020), Discrete generalized Burr-Hatke model with properties, different estimation methods and characterizations by Yousof et al. (2021), The discrete inverse Burr model with characterizations, properties, applications to count data, Bayesian and non-Bayesian estimations by Chesneau et al. (2022), among others. Numerous current families can benefit from the use of a variety of practical discretization techniques (see Hamedani et al. (2018a,b, 2019), Cordeiro et al. (2018), Korkmaz et al. (2018a,b), and Nascimento et al. (2019)).

Although there are many discrete distributions in statistical literature, the presence of discrete G families is still rare, the fact is there are not many discrete G families in the statistical literature. Therefore, we can limit these families to the following: discrete Gompertz G family of distributions by Eliwa et al. (2020), discrete Rayleigh G by Aboraya et al. (2020), discrete Weibull G family by Ibrahim et al. (2021), A discrete analogue of odd Weibull-G family of distributions with some properties, Bayesian and non-Bayesian estimation and count data modeling by El-Morshedy et al. (2022). and A discrete exponential generalized-G family of distributions with mathematical Properties, Bayesian and non-Bayesian estimators for modeling engineering, medical, and agriculture count data. by Eliwa et al. (2022). Therefore, we are excited to present this new family, study it theoretically and practically, and present a deep applied study of it based on different data in its form and nature. The following motivations are behind our decision to introduce the DGR-G family:

I. Creating new probability mass functions that can be, among other helpful forms, "symmetric," "asymmetric and bimodal,", "right skewed with a heavy tail," "asymmetric and left skewed," and "symmetric and right skewed." Since the probability of mass function for novel models is so flexible, we may use them to study variety of data environments.

II. Introducing a few new, unique models that use various hazard rate functions, including "decreasing-constant," "constant," "bathtub (U- hazard rate function)" "monotonically decreasing ", "monotonically increasing" and "decreasing-constant"." The distribution's flexibility increases with the number of different failure rate types. The job of many practitioners who may employ the new distribution in statistical modeling and mathematical analysis is made easier by these forms. We have paid a lot of attention to the issue of checking the failure rate function for this specific purpose.

III. The new distribution's flexibility depends on several factors, including the magnitude of the skew coefficient, kurtosis coefficient, failure rate function, and variety in the PMF and failure rate functions. The probability distribution's applicability and efficacy in statistical modeling are also critical in this context. Upon closer inspection, we found that the innovative probability mass function was extremely versatile in these and other areas. This inspired us to conduct a detailed analysis of this probability distribution.

IV. Putting out new discrete models to describe real data that is "over-dispersed," "equal-dispersed," and "under-dispersed." As will be seen, the new discrete family has demonstrated a surprising advantage in modeling various forms of data, regardless of whether they are symmetric or asymmetric or whether they contain outliers or not.

V. Introducing novel discrete models for the analysis of zero-inflated and extreme count data.

VI. Compare the estimating techniques for simulated and real-world data in order to suggest the most appropriate technique in each situation.

VII. The cornerstone of a statistical model known as a zero-inflated model in statistics is a zero-inflated probability distribution, or distribution that allows multiple zero-valued observations. For instance, the number of insurance claims within a community for a specific type of risk would be zero-inflated if people who are unable to file a claim because they have not acquired insurance against the risk. In this work, we are inspired to utilize the novel family instead of the zero-inflated Poisson regression model, which is frequently used to model and forecast zero-inflated count data.

VIII. The new family under the Weibull baseline model produced appropriate results in statistical modeling of the bathtub hazard rate count data, and as a consequence, the new family under the Weibull baseline is advised for modeling the bathtub hazard rate count data. Additionally, the same baseline model may adequately explain the monotonically increasing failure rate count data.

IX. The new family was a suitable alternative to handle zero-inflated medical data with a decreasing failure rate and certain outliers.

X. The new class was a suitable choice for modeling zero-inflated agricultural data that has a decreasing-increasing-decreasing failure rate and contains some outliers.

XI. In fact, we experimentally show that the proposed G family of distributions matches more closely four real data sets than other sixteen extended competitive distributions with three and four parameters.

XII. Regarding the estimation and statistical inference side, other traditional (non-Bayesian) estimating techniques are considered, such as the maximum likelihood estimation, ordinary least square estimation, and weighted-

least square estimation. Also taken into consideration is the Bayesian estimate under the squared error loss function. The traditional Markov chain Monte Carlo simulations are used to contrast the Bayesian and conventional approaches. Four actual data sets are used to demonstrate and debate the applicability of the DGR-G family. Due to the consistent Akaike information criteria, Akaike information criterion, Chi-square, Kolmogorov-Smirnov, and its related P-value, the DGR -G family under the Weibull model case gave a better match than many rival models.

The structure of this work is as follows. In Section 2, a few mathematical characteristics of the DGR-G family are deduced and examined. In Section 3, several characterization findings are presented. Section 4 presents estimation and inference techniques. In Section 5, Markov chain Monte Carlo simulations are used to contrast Bayesian and non-Bayesian estimation techniques. Section 6 deals with four actual data examples for contrasting Bayesian and non-Bayesian estimate techniques. In Section 7, four applications for contrasting the competing discrete models are taken into account. Section 8 gives some concluding remarks.

2.Properties

2.1 Ordinary moments

Theorem 2.1:

Let X be an NNRV, where X ~DGR-G($\pi, \sigma, \underline{\boldsymbol{\Psi}}$) family, then the r^{th} moment of X can be expressed as

$$\mu'_{r,X} = E(X^r) = \sum_{x=1}^{\infty} [x^r - (x-1)^r]\, \pi^{\boldsymbol{H}^2_{\sigma,\underline{\boldsymbol{\Psi}}}(x)}|_{(x\in \boldsymbol{\mathcal{N}}^{\bullet}, \pi\in(0,1) \text{ and } r=1,2,3,\ldots)}. \quad (5)$$

Proof: Since

$$\mu'_{r,X} = E(X^r) = \sum_{x=0}^{\infty} x^r\, S_{\pi,\sigma,\underline{\boldsymbol{\Psi}}}(x).$$

Then,

$$\mu'_{r,X} = E(X^r) = \sum_{x=0}^{\infty} x^r \left[\pi^{\boldsymbol{H}^2_{\sigma,\underline{\boldsymbol{\Psi}}}(x)} - \pi^{\boldsymbol{H}^2_{\sigma,\underline{\boldsymbol{\Psi}}}(x+1)}\right]$$

$$= \sum_{x=1}^{\infty} [x^r - (x-1)^r]\, S_{\pi,\sigma,\underline{\boldsymbol{\Psi}}}(x-1)$$

$$= \sum_{x=1}^{\infty} [x^r - (x-1)^r]\, \pi^{\boldsymbol{H}^2_{\sigma,\underline{\boldsymbol{\Psi}}}(x)}|_{(x\in \boldsymbol{\mathcal{N}}^{\bullet}, \pi\in(0,1) \text{ and } r=1,2,3,\ldots)}.$$

Then, using (5), the mean ($\mu'_{1,X}$), and $\mu'_{2,X}$ can be respectively written as

$$\mu'_{1,X} = E(X) = \sum_{x=1}^{\infty} \pi^{\boldsymbol{H}^2_{\sigma,\underline{\boldsymbol{\Psi}}}(x)}\,|_{(x\in \boldsymbol{\mathcal{N}}^{\bullet}, \pi\in(0,1) \text{ and } r=1)},$$

and

$$\mu'_{2,X} = E(X^2) = \sum_{x=1}^{\infty} (2x-1)\, \pi^{\boldsymbol{H}^2_{\sigma,\underline{\boldsymbol{\Psi}}}(x)}|_{(x\in \boldsymbol{\mathcal{N}}^{\bullet}, \pi\in(0,1) \text{ and } r=2)}.$$

2.2 Central moments

The r^{th} central moment of X, say $\mu_{r,X}$, is

$$\mu_{r,X} = E(X - \mu'_{1,X})^r = \sum_{k=0}^{r} (-\mu'_1)^k \binom{r}{k} \mu'_{r-k}|_{\left(|_{(x\in \boldsymbol{\mathcal{N}}^{\bullet}, \pi\in(0,1) \text{ and } r=1,2,3,\ldots)}\right)}.$$

So, the variance ($V(X)$) from

$$E\left(X - \mu'_{1,X}\right)^2 = \mu \sum_{k=0}^{r} (-\mu'_1)^k \binom{r}{k} \mu'_{2-k,X}|_{\left(|_{(x\in \boldsymbol{\mathcal{N}}^{\bullet}, \pi\in(0,1) \text{ and } r=2)}\right)},$$

can be derived using the ordinary moments

$$\mu_{2,X} = V(X) = \mu'_{2,X} - \left(\mu'_{1,X}\right)^2 = \sum_{x=1}^{\infty} (2x-1)\, \pi^{\boldsymbol{H}^2_{\sigma,\underline{\boldsymbol{\Psi}}}(x)} - \left(\mu'_{1,X}\right)^2|_{(x\in \boldsymbol{\mathcal{N}}^{\bullet}, \pi\in(0,1) \text{ and } r=2)}.$$

The DisIx or the variance to mean ratio (VMR) of the DGR-G family can be derived as

$$\text{DisIx}(X) = \frac{\sum_{x=1}^{\infty}(2x-1)\,\pi^{\boldsymbol{H}^2_{\sigma,\underline{\boldsymbol{\Psi}}}(x)}}{\sum_{x=1}^{\infty}\pi^{\boldsymbol{H}^2_{\sigma,\underline{\boldsymbol{\Psi}}}(x)}} - \sum_{x=1}^{\infty}\pi^{\boldsymbol{H}^2_{\sigma,\underline{\boldsymbol{\Psi}}}(x)}\,|_{(x\in\boldsymbol{\mathcal{N}}^{\bullet}\text{ and }\pi\in(0,1))}.$$

When describing the distribution of events or objects in time or space, the VMR is utilized. The VMR is approximately 1 if the distribution is random, that is, if it can be represented by the Poisson process or one of its multidimensional counterparts. Greater results (VMR >1) indicate the presence of geographical or temporal clusters or "clumps." Smaller values (1> VMR) represent a distribution that is more equal or uniform than random, or mutual "avoidance" of occurrences or objects in time or space. The essential characteristic of the Poisson distribution—that the variance and mean are equal—gives rise to these characteristics of VMR. The Variance/Mean Ratio test makes use of the VMR.

2.3 The moment and cumulant generating function (MGF & CGF)

***Theorem 2.2*:**

Let X be an NNRV, where X ~DGR-G($\pi, \sigma, \underline{\boldsymbol{\Psi}}$) family, then the MGF of X can be obtained as

$$M_X(t) = 1 + \sum_{x=1}^{\infty}\{exp(tX) - exp[t(X-1)]\}\,\pi^{\boldsymbol{H}^2_{\sigma,\underline{\boldsymbol{\Psi}}}(x)}|_{(x\in\boldsymbol{\mathcal{N}}^{\bullet},\pi\in(0,1)\text{ and }r=1,2,3,\ldots)}. \quad (6)$$

Proof:

The MGF of our NNRV X can be derived from

$$M_X(t) = \sum_{x=0}^{\infty} exp(tX)\,S_{\pi,\underline{\boldsymbol{\Psi}}}(x).$$

Using (3) we have

$$M_X(t) = \sum_{x=0}^{\infty} exp(tX)\left[\pi^{\boldsymbol{H}^2_{\sigma,\underline{\boldsymbol{\Psi}}}(x)} - \pi^{\boldsymbol{H}^2_{\sigma,\underline{\boldsymbol{\Psi}}}(x+1)}\right],$$

then

$$M_X(t) = 1 + \sum_{x=1}^{\infty}\{exp(tX) - exp[t(X-1)]\}\,\pi^{\boldsymbol{H}^2_{\sigma,\underline{\boldsymbol{\Psi}}}(x)}|_{(x\in\boldsymbol{\mathcal{N}}^{\bullet},\pi\in(0,1)\text{ and }r=1,2,3,\ldots)}.$$

The first r derivatives of (6), with respect to $t|t=0$, yield the first r raw moments, i.e.,

$$\mu'_{r,X} = E(X^r) = \frac{d^r}{dt^r}M_X(t)|_{(t=0\text{ and }r=1,2,3,\ldots)},$$

where

$$\mu'_{1,X} = E(X) = \frac{d}{dt}M_X(t)|_{t=0} = \sum_{x=1}^{\infty}\pi^{\boldsymbol{H}^2_{\sigma,\underline{\boldsymbol{\Psi}}}(x)}\,|_{(x\in\boldsymbol{\mathcal{N}}^{\bullet},\pi\in(0,1)\text{ and }r=1)},$$

$$\mu'_{2,X} = E(X^2) = \frac{d^2}{dt^2}M_X(t)|_{(t=0)} = \sum_{x=1}^{\infty}(2x-1)\,\pi^{\boldsymbol{H}^2_{\sigma,\underline{\boldsymbol{\Psi}}}(x)}|_{(x\in\boldsymbol{\mathcal{N}}^{\bullet},\pi\in(0,1)\text{ and }r=2)},$$

$$\mu'_{3,X} = E(X^3) = \frac{d^3}{dt^3}M_X(t)|_{(t=0)} = \sum_{x=1}^{\infty}[3x(x-1)+1]\,\pi^{\boldsymbol{H}^2_{\sigma,\underline{\boldsymbol{\Psi}}}(x)}|_{(x\in\boldsymbol{\mathcal{N}}^{\bullet},\pi\in(0,1)\text{ and }r=3)},$$

and

$$\mu'_{4,X} = E(X^4) = \frac{d^4}{dt^4}M_X(t)|_{(t=0)} = \sum_{x=1}^{\infty}[x^4-(x-1)^4]\,\pi^{\boldsymbol{H}^2_{\sigma,\underline{\boldsymbol{\Psi}}}(x)}|_{(x\in\boldsymbol{\mathcal{N}}^{\bullet},\pi\in(0,1)\text{ and }r=4)}.$$

The CGF is the logarithm of the MGF. Thus, r^{th} cumulant, say $\kappa_{r,X}$, can be obtained from

$$\kappa_{r,X} = \frac{d^r}{dt^r}log[M_X(t)]\,|_{(t=0,\text{ and }r=1,2,3,\ldots)}.$$

The 1st cumulant ($\kappa_{1,X}$) is the mean ($\mu'_{1,X}$), the 2nd cumulant ($\kappa_{2,X}$) is the variance ($Var(X)$), and the 3rd cumulant ($\kappa_{3,X}$) is the same as the 3rd central moment $\kappa_{3,X} = \mu_{3,X}$, that being $\kappa_{1,X} = \mu'_{1,X} = E(X), \kappa_{2,X} = \mu_{2,X} = \mu'_{2,X} - \mu'^2_{1,X}$ and $\kappa_{3,X} = \mu_{3,X} = \mu'_{3,X} - 3\mu'_{2,X}\mu'_{1,X} + 2\mu'^3_{1,X}$. However the 4th and higher order cumulants are not equal to the central moments. In certain circumstances, theoretical solutions to issues that use cumulants instead of moments are more

straightforward, especially when there are two or more statistically independent RVs, the r^{th} order cumulant of their sum is equal to the sum of their r^{th} order cumulants. Moreover, the cumulants can also be obtained from

$$\kappa_{r,X}|_{r\geq 1} = \mu'_{r,X} - \sum_{k=0}^{r-1} \binom{r-1}{k-1} \mu'_{r-k,X}\kappa_{k,X}.$$

It is possible to write the probability generating function as

$$P_X(s) = 1 + \sum_{x=1}^{\infty} \left(1 - \frac{1}{s}\right) s^x \pi^{\boldsymbol{H}^2_{\sigma,\underline{\boldsymbol{\Psi}}}(x)}|_{(x\in\mathcal{N}^{\bullet},\pi\in(0,1) \text{ and } r=1,2,3,\ldots)}.$$

It has several applications in a variety of disciplines, including computer science, information theory, quantum information, survival analysis, and econometrics. It is possible to develop and research the measure of variation of the uncertainty of the random variable X in a separate article. It is possible to derive and use L-moments in a manner similar to how ordinary moments are. However, a linear combination of the order statistics may also be used to estimate the L-moments. The L-moments are there whenever the distribution's mean is present. It is possible to construct explicit formulas for the L-moments as infinitely many weighted linear combinations of the appropriate DGR-G order statistics' means. The predicted order statistics may be written as a linear function of the L-moments, which can be described as

$$\xi_{r,X} = \frac{1}{r}\sum_{\varsigma=0}^{r-1} E\left(X_{r-\varsigma:\varsigma}\right)\mathcal{W}(r,\varsigma)\,|_{\,r\geq 1},$$

where

$$\mathcal{W}(r,\varsigma) = \binom{r-1}{\varsigma}(-1)^{\varsigma}.$$

The first four L-moments are given by:

$$\xi_{1,X} = \xi_1(X) = \mathbf{E}(X_{1:1}),$$

$$\xi_{2,X} = \xi_2(X) = \frac{1}{2}\mathbf{E}(X_{2:2} - X_{1:2}),$$

$$\xi_{3,X} = \xi_3(X) = \frac{1}{3}\mathbf{E}(X_{3:3} - 2X_{2:3} + X_{1:3})$$

and

$$\xi_{4,X} = \xi_4(X) = \frac{1}{4}\mathbf{E}(X_{4:4} - 3X_{3:4} + 3X_{2:4} - X_{1:4}).$$

For the Weibull base line model and based on (3), the PMF of the discrete generated Rayleigh Weibull (DGR-W) model can be expressed as

$$f_{\pi,\sigma,\theta}(x) = \pi^{\boldsymbol{H}^2_{\sigma,\,\theta}(x)} - \pi^{\boldsymbol{H}^2_{\sigma,\,\theta}(x+1)}\ |_{(x\in\mathcal{N}^{\bullet},\pi\in(0,1) \text{ and } \sigma,\theta>0)},$$

$$\boldsymbol{H}^2_{\sigma,\,\theta}(x) = \frac{\left[1-\exp\left(-x^{\theta}\right)\right]^{\sigma}}{1-\left[1-\exp\left(-x^{\theta}\right)\right]^{\sigma}}$$

and

$$\boldsymbol{H}^2_{\sigma,\,\theta}(x+1) = \frac{\left\{1-\exp\left[-(x+1)^{\theta}\right]\right\}^{\sigma}}{1-\left\{1-\exp\left[-(x+1)^{\theta}\right]\right\}^{\sigma}}.$$

Clearly, when $\theta = 1$, the DGR-W model reduced to the DGR-exponential model. The PMF of the DGR-W model is plotted in Figure 1 for a variety of parameter values. Figure 2 displays many charts of the DGR-W model's HRF for various parameter values. Based on Figure 1, we conclude that the PMF of the DGR-W can be "right skewed with one peak", "right skewed with two peaks (right skewed and bimodal)", "symmetric mass function" "left skewed with one peak". Based on Figure 2, we see that the HRF of the DGR-W can be "monotonically decreasing," "upside down," "monotonically increasing," "constant," "decreasing-constant," and "decreasing-constant-increasing (U- hazard rate function)".

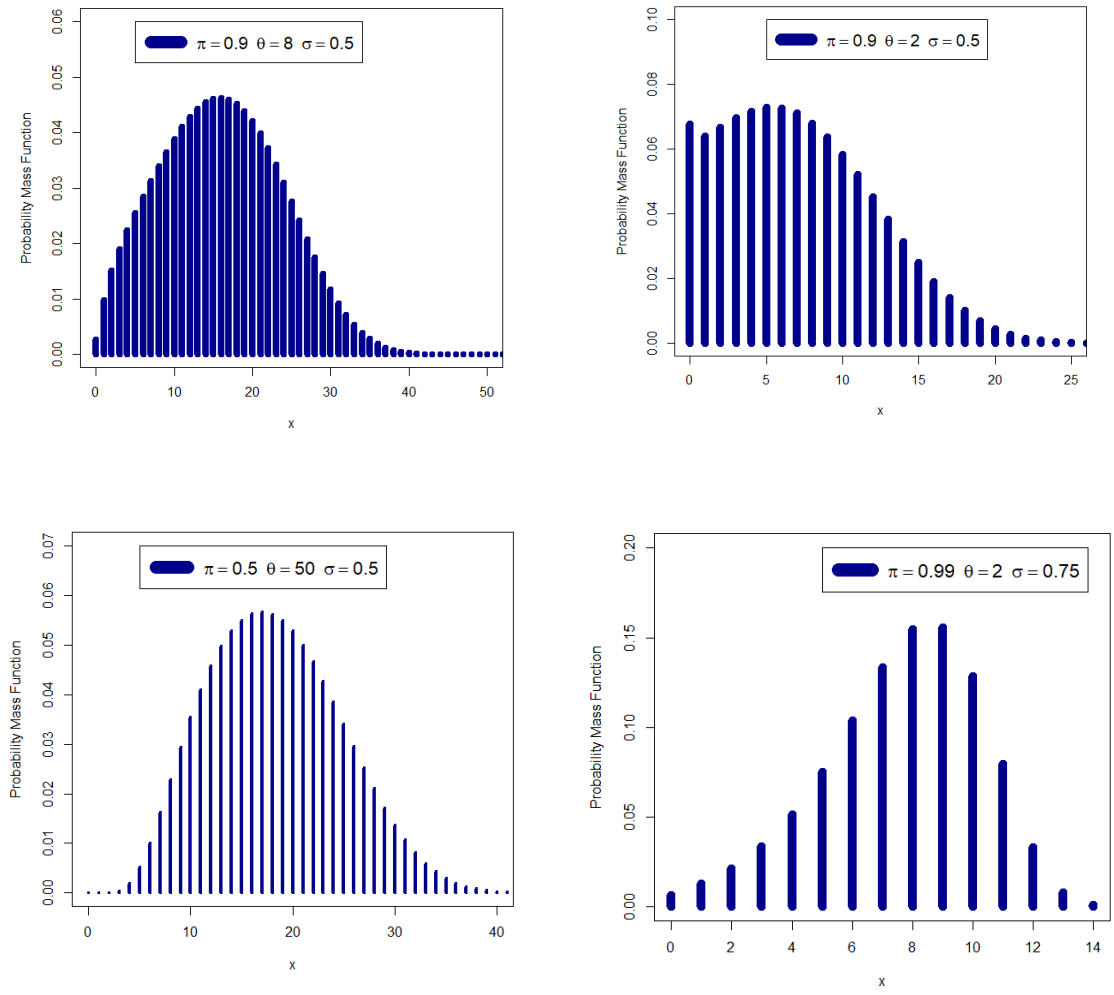

Figure 1: The PMF of the DGR-W for different parameters values.

The size of the skew coefficient, kurtosis coefficient, failure rate function, and variety of the PMF and failure rate functions are some of the aspects that affect how flexible the new distribution is. The usefulness and effectiveness of the probability distribution in statistical modeling are also crucial in this situation. When we looked more closely, we discovered that the novel probability mass function was quite flexible in these and other areas. This motivated us to analyze this probability distribution in great depth.

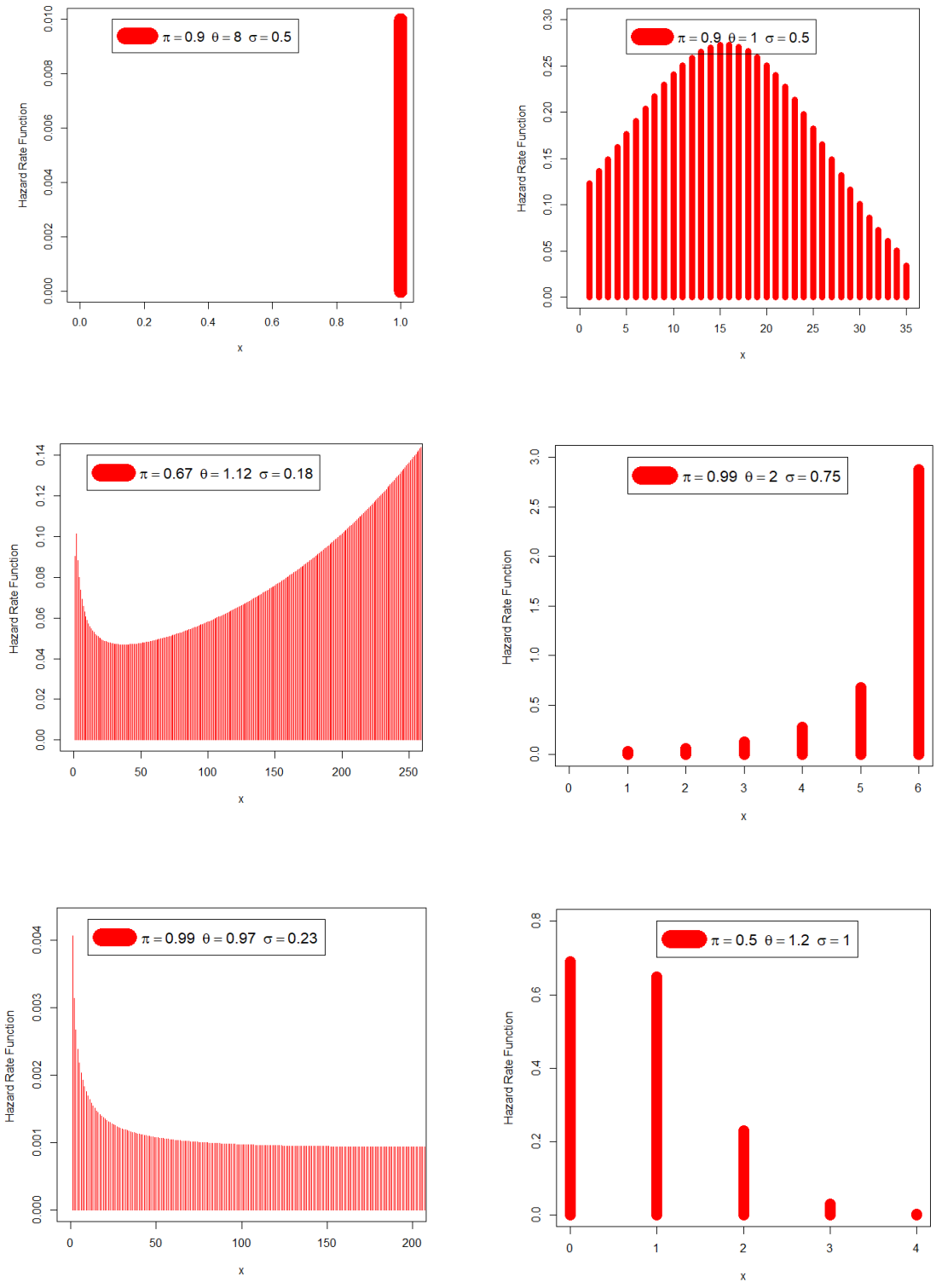

Figure 2: The HRF of the DGR-W for different parameters values.

3. Characterizations Results

In this Section, we present our characterizations of the DGR-G distribution in two subsections: (i) in terms of the truncated moments of certain function of the random variable, (ii) based on the hazard function.

3.1 Characterizations Based on Conditional Expectation

Proposition 3.1.1. Let $X:\Omega \to N_{[0]}$ be a random variable. The PMF of X is (3) if and only if

$$E\left\{\left[\pi^{H^2_{\sigma,\underline{\Psi}}(X)}+\pi^{H^2_{\sigma,\underline{\Psi}}(X+1)}\right] \mid X>k\right\}=\pi^{H^2_{\sigma,\underline{\Psi}}(k+1)}. \tag{7}$$

Proof. If X has PMF (3), then for $k \in N_{[0]}$, the left-hand side of (7), using telescoping sum formula, will be

$$\left(1-F_{\pi,\sigma,\underline{\Psi}}(k)\right)^{-1}\sum_{x=k+1}^{\infty}\left\{\pi^{2H^2_{\sigma,\underline{\Psi}}(x)}-\pi^{2H^2_{\sigma,\underline{\Psi}}(x+1)}\right\}=\pi^{-\left\{\frac{G(k+1)^{\sigma}}{1-G(k+1)^{\sigma}}\right\}^2}\sum_{x=k+1}^{\infty}\left\{\pi^{H^2_{\sigma,\underline{\Psi}}(x)}-\pi^{H^2_{\sigma,\underline{\Psi}}(x+1)}\right\}$$
$$=\pi^{-H^2_{\sigma,\underline{\Psi}}(k+1)}\left\{\pi^{2H^2_{\sigma,\underline{\Psi}}(k+1)}\right\}=\pi^{H^2_{\sigma,\underline{\Psi}}(k+1)}.$$

Conversely, if (7) holds, then

$$\sum_{x=k+1}^{\infty}\left\{\begin{bmatrix}\pi^{H^2_{\sigma,\underline{\Psi}}(x)}\\+\pi^{H^2_{\sigma,\underline{\Psi}}(x+1)}\end{bmatrix}f_{\pi,\sigma,\underline{\Psi}}(x)\right\}=\left(1-F_{\pi,\sigma,\underline{\Psi}}(k)\right)\pi^{H^2_{\sigma,\underline{\Psi}}(k+1)}=\begin{pmatrix}1-F_{\pi,\sigma,\underline{\Psi}}(k+1)\\+f_{\pi,\sigma,\underline{\Psi}}(k+1)\end{pmatrix}\pi^{H^2_{\sigma,\underline{\Psi}}(k+1)}. \tag{8}$$

From (8), we also have

$$\sum_{x=k+2}^{\infty}\left\{\left[\pi^{H^2_{\sigma,\underline{\Psi}}(x)}+\pi^{H^2_{\sigma,\underline{\Psi}}(k+1)}\right]f_{\pi,\sigma,\underline{\Psi}}(x)\right\}=\left(1-F_{\pi,\sigma,\underline{\Psi}}(k+1)\right)\pi^{H^2_{\sigma,\underline{\Psi}}(k+2)}. \tag{9}$$

Now, subtracting (9) from (8), yields

$$\left[\pi^{H^2_{\sigma,\underline{\Psi}}(k+1)}+\pi^{H^2_{\sigma,\underline{\Psi}}(k+2)}\right]f(k+1)=\left(1-F(k+1)\right)\left\{\pi^{H^2_{\sigma,\underline{\Psi}}(k+1)}-\pi^{H^2_{\sigma,\underline{\Psi}}(k+2)}\right\}+f_{\pi,\sigma,\underline{\Psi}}(k+1)\pi^{H^2_{\sigma,\underline{\Psi}}(k+1)}.$$

From the above equality, we have

$$\frac{f_{\pi,\sigma,\underline{\Psi}}(k+1)}{1-F_{\pi,\sigma,\underline{\Psi}}(k+1)}=\frac{\pi^{H^2_{\sigma,\underline{\Psi}}(k+1)}-\pi^{H^2_{\sigma,\underline{\Psi}}(k+2)}}{\pi^{H^2_{\sigma,\underline{\Psi}}(k+2)}}=\frac{\pi^{H^2_{\sigma,\underline{\Psi}}(k+1)}}{\pi^{H^2_{\sigma,\underline{\Psi}}(k+2)}}-1,$$

which is the hazard function, (4) corresponding to the PMF (3), so X has PMF (3) .

3.2. Characterizations of distributions based on hazard function

Proposition 3.2.1. Let $X:\Omega \to N_{[0]}$ be a random variable. The PMF of X is (3) if and only if its hazard function satisfies the difference equation

$$h_{\pi,\sigma,\underline{\Psi}}(k+1)-h_{\pi,\sigma,\underline{\Psi}}(k)=\frac{\pi^{H^2_{\sigma,\underline{\Psi}}(k+1)}}{\pi^{H^2_{\sigma,\underline{\Psi}}(k+2)}}-\frac{\pi^{H^2_{\sigma,\underline{\Psi}}(k)}}{\pi^{H^2_{\sigma,\underline{\Psi}}(k+1)}},\quad k\in N, \tag{10},$$

with the initial condition $h_{\pi,\sigma,\underline{\Psi}}(0)=\frac{\pi^{H^2_{\sigma,\underline{\Psi}}(0)}}{\pi^{H^2_{\sigma,\underline{\Psi}}(1)}}-1.$

Proof. If X has PMF (3), then clearly (10) holds. Now, if (10) holds, then for every $x \in N$, we have

$$\sum_{k=0}^{x-1}\left\{h_{\pi,\sigma,\underline{\Psi}}(k+1)-h_{\pi,\sigma,\underline{\Psi}}(k)\right\}=\sum_{k=0}^{x-1}\left\{\frac{\pi^{H^2_{\sigma,\underline{\Psi}}(k+1)}}{\pi^{H^2_{\sigma,\underline{\Psi}}(k+2)}}-\frac{\pi^{H^2_{\sigma,\underline{\Psi}}(k)}}{\pi^{H^2_{\sigma,\underline{\Psi}}(k+1)}}\right\}=\frac{\pi^{H^2_{\sigma,\underline{\Psi}}(x+1)}}{\pi^{\left\{\frac{G(x+2)^{\sigma}}{1-G(x+2)^{\sigma}}\right\}^2}}-\frac{\pi^{H^2_{\sigma,\underline{\Psi}}(0)}}{\pi^{H^2_{\sigma,\underline{\Psi}}(1)}},$$

or

$$h_{\pi,\sigma,\underline{\Psi}}(x)-h_{\pi,\sigma,\underline{\Psi}}(1)=\frac{\pi^{H^2_{\sigma,\underline{\Psi}}(x+1)}}{\pi^{\left\{\frac{G(x+2)^{\sigma}}{1-G(x+2)^{\sigma}}\right\}^2}}-\frac{\pi^{H^2_{\sigma,\underline{\Psi}}(0)}}{\pi^{H^2_{\sigma,\underline{\Psi}}(1)}},$$

or, in view of the initial condition

$$h_{\pi,\sigma,\underline{\Psi}}(x)=\frac{\pi^{H^2_{\sigma,\underline{\Psi}}(x+1)}}{\pi^{H^2_{\sigma,\underline{\Psi}}(x+2)}}-1,\quad x\in N_{[0]},$$

which is the hazard function (4), corresponding to the PMF (3).

4.Estimation and inference

The various estimating techniques, including classical and Bayesian techniques, will be covered in this section. There are many different types of classical techniques, some of which are based on maximizing theory and others on minimization theory. In any event, as will be thoroughly demonstrated in theory and practice, the classical approaches

generally differ from the Bayes method in origin and methodology of estimation. This section's two subsections discuss Bayesian and non-Bayesian estimating methods. The first paragraph takes into account eight non-Bayesian estimating approaches, including the MLE, OLSE, and WLSE methods. The second portion then takes into account the Bayesian estimation technique using the well-known squared error loss function (SELF).

4.1 Non-Bayesian estimation methods

4.1.1 The MLE method

A statistical method known as maximum likelihood estimation (MLE) is used to estimate the unknown parameters of a probability distribution that has been assumed in light of certain observed data. To do this, a likelihood function is maximized to increase the probability of the observed data under the presumptive statistical model. The parameter space position where the likelihood function is maximized is known as the maximum likelihood estimate. A common method for drawing statistical conclusions is maximum likelihood because of its adaptive and transparent justification. If the likelihood function is differentiable, then maxima can be determined using the derivative test. For instance, the ordinary least squares estimator increases the likelihood of the linear regression model, enabling in some cases to explicitly solve the first-order conditions of the likelihood function. However, it will frequently be necessary to utilize numerical methods to ascertain the maximum of the probability function. From the perspective of Bayesian inference, MLE is often equivalent to maximum of a posteriori (MAP) estimates under a uniform prior distribution on the parameters. When likelihood serves as the goal function in frequentist inference, MLE is a special illustration of an extremum estimator. Let $X_1, X_2, \ldots, X_n$ be a random sample (RS) from the DGR-G distribution. The log-likelihood function is given by

$$\ell = \ell\left(\pi, \sigma, \underline{\boldsymbol{\Psi}}_j\right) = \sum_{i=1}^{n} \log\left[\pi^{\boldsymbol{H}^2_{\sigma,\underline{\boldsymbol{\Psi}}_j}(x_{i:n})} - \pi^{\boldsymbol{H}^2_{\sigma,\underline{\boldsymbol{\Psi}}_j}(x_{i:n}+1)}\right]|_{(\pi\in(0,1),\ j=1,2,..,p \text{ and } x_{i:n}\in\boldsymbol{\mathcal{N}}^{\bullet})},$$

which can be maximized either using the statistical programs or by solving the nonlinear system obtained from $\ell(\pi, \sigma, \underline{\boldsymbol{\Psi}}_j)$ via differentiation. The score vector components are given below where

$$U\left(\pi, \sigma, \underline{\boldsymbol{\Psi}}_j\right) = \left(\partial\ell(\pi, \sigma, \underline{\boldsymbol{\Psi}}_j)/\partial\pi, \partial\ell(\pi, \sigma, \underline{\boldsymbol{\Psi}}_j)/\partial\sigma, \partial\ell(\pi, \sigma, \underline{\boldsymbol{\Psi}}_j)/\partial\underline{\boldsymbol{\Psi}}_j\right)^T,$$

$$\partial\ell(\pi, \sigma, \underline{\boldsymbol{\Psi}}_j)/\partial\pi = \sum_{i=1}^{n} \frac{\boldsymbol{H}^2_{\sigma,\underline{\boldsymbol{\Psi}}_j}(x_{i:n})\pi^{\left[\boldsymbol{H}^2_{\sigma,\underline{\boldsymbol{\Psi}}_j}(x_{i:n})\right]-1} - \boldsymbol{H}^2_{\sigma,\underline{\boldsymbol{\Psi}}_j}(x_{i:n}+1)\pi^{\left[\boldsymbol{H}^2_{\sigma,\underline{\boldsymbol{\Psi}}_j}(x_{i:n}+1)\right]-1}}{\pi^{\boldsymbol{H}^2_{\sigma,\underline{\boldsymbol{\Psi}}_j}(x_{i:n})} - \pi^{\boldsymbol{H}^2_{\sigma,\underline{\boldsymbol{\Psi}}_j}(x_{i:n}+1)}},$$

$$\partial\ell(\pi, \sigma, \underline{\boldsymbol{\Psi}}_j)/\partial\sigma = \sum_{i=1}^{n} \frac{\frac{\partial\boldsymbol{H}^2_{\sigma,\underline{\boldsymbol{\Psi}}_j}(x_{i:n})}{\partial\sigma}\pi^{\boldsymbol{H}^2_{\underline{\boldsymbol{\Psi}}_j}(x_{i:n})}\ln(\pi) - \frac{\partial\boldsymbol{H}^2_{\sigma,\underline{\boldsymbol{\Psi}}_j}(x_{i:n}+1)}{\partial\sigma}\pi^{\boldsymbol{H}^2_{\underline{\boldsymbol{\Psi}}_j}(x_{i:n}+1)}\ln(\pi)}{\pi^{\boldsymbol{H}^2_{\sigma,\underline{\boldsymbol{\Psi}}_j}(x_{i:n})} - \pi^{\boldsymbol{H}^2_{\sigma,\underline{\boldsymbol{\Psi}}_j}(x_{i:n}+1)}}$$

and

$$\partial\ell(\pi, \sigma, \underline{\boldsymbol{\Psi}}_j)/\partial\underline{\boldsymbol{\Psi}}_j = \sum_{i=1}^{n} \frac{\frac{\partial\boldsymbol{H}^2_{\sigma,\underline{\boldsymbol{\Psi}}_j}(x_{i:n})}{\partial\underline{\boldsymbol{\Psi}}_j}\pi^{\boldsymbol{H}^2_{\underline{\boldsymbol{\Psi}}_j}(x_{i:n})}\ln(\pi) - \frac{\partial\boldsymbol{H}^2_{\sigma,\underline{\boldsymbol{\Psi}}_j}(x_{i:n}+1)}{\partial\underline{\boldsymbol{\Psi}}_j}\pi^{\boldsymbol{H}^2_{\underline{\boldsymbol{\Psi}}_j}(x_{i:n}+1)}\ln(\pi)}{\pi^{\boldsymbol{H}^2_{\sigma,\underline{\boldsymbol{\Psi}}_j}(x_{i:n})} - \pi^{\boldsymbol{H}^2_{\sigma,\underline{\boldsymbol{\Psi}}_j}(x_{i:n}+1)}}|_{(j=1,2,..,p)},$$

where

$$\frac{\partial}{\partial\sigma}\boldsymbol{H}^2_{\sigma,\underline{\boldsymbol{\Psi}}_j}(x_{i:n}) = 2\boldsymbol{H}_{\sigma,\underline{\boldsymbol{\Psi}}_j}(x_{i:n})\frac{\partial}{\partial\sigma}\boldsymbol{H}_{\sigma,\underline{\boldsymbol{\Psi}}_j}(x_{i:n}),$$

$$\frac{\partial}{\partial\sigma}\boldsymbol{H}^2_{\sigma,\underline{\boldsymbol{\Psi}}_j}(x_{i:n}+1) = 2\boldsymbol{H}_{\sigma,\underline{\boldsymbol{\Psi}}_j}(x_{i:n}+1)\frac{\partial}{\partial\sigma}\boldsymbol{H}_{\sigma,\underline{\boldsymbol{\Psi}}_j}(x_{i:n}+1),$$

$$\frac{\partial}{\partial\underline{\boldsymbol{\Psi}}_j}\boldsymbol{H}^2_{\sigma,\underline{\boldsymbol{\Psi}}_j}(x_{i:n}) = 2\boldsymbol{H}_{\sigma,\underline{\boldsymbol{\Psi}}_j}(x_{i:n})\frac{\partial}{\partial\underline{\boldsymbol{\Psi}}_j}\boldsymbol{H}_{\sigma,\underline{\boldsymbol{\Psi}}_j}(x_{i:n}),$$

and

$$\frac{\partial}{\partial\underline{\boldsymbol{\Psi}}_j}\boldsymbol{H}^2_{\sigma,\underline{\boldsymbol{\Psi}}_j}(x_{i:n}+1) = 2\boldsymbol{H}_{\sigma,\underline{\boldsymbol{\Psi}}_j}(x_{i:n}+1)\frac{\partial}{\partial\underline{\boldsymbol{\Psi}}_j}\boldsymbol{H}_{\sigma,\underline{\boldsymbol{\Psi}}_j}(x_{i:n}+1).$$

Setting

$$0 = \frac{\partial\ell\left(\pi, \sigma, \underline{\boldsymbol{\Psi}}_j\right)}{\partial\pi} = \frac{\partial\ell\left(\pi, \sigma, \underline{\boldsymbol{\Psi}}_j\right)}{\partial\sigma} = \frac{\partial\ell\left(\pi, \sigma, \underline{\boldsymbol{\Psi}}_j\right)}{\partial\underline{\boldsymbol{\Psi}}_j}$$

and solving them simultaneously yields the MLEs for the parameters of the DGR-G family. The Newton-Raphson algorithms is employed for obtaining the numerical solutions in such cases.

41.2 The CVME method

The CVME of the parameters $\pi, \sigma, \underline{\boldsymbol{\Psi}}_j$ are obtained via minimizing the following expression with respect to π, σ and $\underline{\boldsymbol{\Psi}}_j$ respectively, where

$$CVM_{(\pi,\sigma,\underline{\boldsymbol{\Psi}}_j)} = \frac{1}{12}n^{-1} + \sum_{i=1}^{n}\left[F_{\pi,\sigma,\underline{\boldsymbol{\Psi}}_j}(x_{i:n}) - c_{(i,n)}^{[1]}\right]^2 |_{(\pi\in(0,1) \text{ and } x_{i:n}\in\mathcal{N}^{\bullet})},$$

and where $c_{(i,n)}^{[1]} = \frac{2i-1}{2n}$ and

$$CVM_{(\pi,\sigma,\underline{\boldsymbol{\Psi}}_j)} = \sum_{i=1}^{n}\left[1 - \pi^{\boldsymbol{H}_{\sigma,\underline{\boldsymbol{\Psi}}_j}^2(x_{i:n}+1)} - c_{(i,n)}^{[1]}\right]^2.$$

The, CVMEs are obtained by solving the following two non-linear equations

$$0 = \sum_{i=1}^{n}\left(1 - \pi^{\boldsymbol{H}_{\sigma,\underline{\boldsymbol{\Psi}}_j}^2(x_{i:n}+1)} - c_{(i,n)}^{[1]}\right)\varpi_{(\pi)}(x_{i:n}+1,\pi,\sigma,\underline{\boldsymbol{\Psi}}_j),$$

$$0 = \sum_{i=1}^{n}\left(1 - \pi^{\boldsymbol{H}_{\sigma,\underline{\boldsymbol{\Psi}}_j}^2(x_{i:n}+1)} - c_{(i,n)}^{[1]}\right)\varpi_{(\sigma)}(x_{i:n}+1,\pi,\sigma,\underline{\boldsymbol{\Psi}}_j),$$

and

$$0 = \sum_{i=1}^{n}\left(1 - \pi^{\boldsymbol{H}_{\sigma,\underline{\boldsymbol{\Psi}}_j}^2(x_{i:n}+1)} - c_{(i,n)}^{[1]}\right)\varpi_{(\underline{\boldsymbol{\Psi}}_j)}(x_{i:n}+1,\pi,\sigma,\underline{\boldsymbol{\Psi}}_j),$$

where

$$\varpi_{(\pi)}(x_{i:n}+1,\pi,\sigma,\underline{\boldsymbol{\Psi}}_j) = \partial F_{\pi,\sigma,\underline{\boldsymbol{\Psi}}_j}(x_{i:n})/\partial\pi\ ,$$
$$\varpi_{(\pi)}(x_{i:n}+1,\pi,\sigma,\underline{\boldsymbol{\Psi}}_j) = \partial F_{\pi,\sigma,\underline{\boldsymbol{\Psi}}_j}(x_{i:n})/\partial\sigma$$

and

$$\varpi_{(\underline{\boldsymbol{\Psi}}_j)}(x_{i:n}+1,\pi,\sigma,\underline{\boldsymbol{\Psi}}_j) = \partial F_{\pi,\sigma,\underline{\boldsymbol{\Psi}}_j}(x_{i:n})/\partial\underline{\boldsymbol{\Psi}}_j$$

are the first partial derivatives of the CDF of DGR-G distribution with respect to π, σ and $\underline{\boldsymbol{\Psi}}_j$ respectively.

4.1.3 OLSE method

Geometrically, this is described as the sum of the squared distances, measured parallel to the axis of the dependent variable, between each data point in the set and its corresponding point on the regression surface. The better the model fits the data, the lesser the differences. The resulting estimator may be expressed by a simple formula, especially in the case of a basic linear regression when there is only one regressor on the right side of the regression equation. Let $F_{\pi,\sigma,\underline{\boldsymbol{\Psi}}_j}(x_{i:n})$ denote the CDF of DGR-G model and let $X_1 < X_2 < \cdots < X_n$ be the n ordered RS. The OLSEs are obtained upon minimizing

$$OLSE_{(\pi,\sigma,\underline{\boldsymbol{\Psi}}_j)} = \sum_{i=1}^{n}\left[F_{\pi,\sigma,\underline{\boldsymbol{\Psi}}_j}(x_{i:n}) - c_{(i,n)}^{[2]}\right]^2,$$

then, we have

$$OLSE_{(\pi,\sigma,\underline{\boldsymbol{\Psi}}_j)} = \sum_{i=1}^{n}\left[1 - \pi^{\boldsymbol{H}_{\sigma,\underline{\boldsymbol{\Psi}}_j}^2(x_{i:n}+1)} - c_{(i,n)}^{[2]}\right]^2,$$

where $c_{(i,n)}^{[2]} = \frac{i}{n+1}$. The LSEs are obtained via solving the following non-linear equations

$$0 = \sum_{i=1}^{n}\left[1 - \pi^{\boldsymbol{H}_{\sigma,\underline{\boldsymbol{\Psi}}_j}^2(x_{i:n}+1)} - c_{(i,n)}^{[2]}\right]\varpi_{(\pi)}(x_{i:n}+1,\pi,\sigma,\underline{\boldsymbol{\Psi}}_j),$$

$$0 = \sum_{i=1}^{n}\left[1 - \pi^{\boldsymbol{H}_{\sigma,\underline{\boldsymbol{\Psi}}_j}^2(x_{i:n}+1)} - c_{(i,n)}^{[2]}\right]\varpi_{(\sigma)}(x_{i:n}+1,\pi,\sigma,\underline{\boldsymbol{\Psi}}_j),$$

and

$$0 = \sum_{i=1}^{n}\left[1 - \pi^{\boldsymbol{H}_{\sigma,\underline{\boldsymbol{\Psi}}_j}^2(x_{i:n}+1)} - c_{(i,n)}^{[2]}\right]\varpi_{(\underline{\boldsymbol{\Psi}}_j)}(x_{i:n}+1,\pi,\sigma,\underline{\boldsymbol{\Psi}}_j),$$

where $\varpi_{(\pi)}(x_{i:n}+1,\pi,\sigma,\underline{\boldsymbol{\Psi}}_j)$, $\varpi_{(\sigma)}(x_{i:n}+1,\pi,\sigma,\underline{\boldsymbol{\Psi}}_j)$ and $\varpi_{(\underline{\boldsymbol{\Psi}}_j)}(x_{i:n}+1,\pi,\sigma,\underline{\boldsymbol{\Psi}}_j)$ defined above.

4.1.4 WLSE method

Weighted least squares (WLS), also known as weighted linear regression (WLR), which integrates information about the variance of the data into the regression, is a generalization of ordinary least squares and linear regression. WLS is yet another generalized least squares variant. The WLSE are obtained by minimizing the function $WLSE_{(\pi,\sigma,\underline{\boldsymbol{\Psi}}_j)}$ with respect to $\pi,\ \sigma$ and $\underline{\boldsymbol{\Psi}}_j$

$$WLSE_{(\pi,\sigma,\underline{\boldsymbol{\Psi}}_j)}=\sum_{i=1}^{n}c_{(i,n)}^{[3]}\left[F_{\pi,\sigma,\underline{\boldsymbol{\Psi}}_j}(x_{i:n})-c_{(i,n)}^{[2]}\right]^2,$$

where $c_{(i,n)}^{[3]}=[(1+n)^2(2+n)]/[i(1+n-i)]$. The WLSEs are obtained by solving

$$0=\sum_{i=1}^{n}c_{(i,n)}^{[3]}\left[1-\pi^{H^2_{\sigma,\underline{\boldsymbol{\Psi}}_j}(x_{i:n}+1)}-c_{(i,n)}^{[2]}\right]\varpi_{(\pi)}(x_{i:n}+1,\pi,\sigma,\underline{\boldsymbol{\Psi}}_j),$$

$$0=\sum_{i=1}^{n}c_{(i,n)}^{[3]}\left[1-\pi^{H^2_{\sigma,\underline{\boldsymbol{\Psi}}_j}(x_{i:n}+1)}-c_{(i,n)}^{[2]}\right]\varpi_{(\sigma)}(x_{i:n}+1,\pi,\sigma,\underline{\boldsymbol{\Psi}}_j),$$

and

$$0=\sum_{i=1}^{n}c_{(i,n)}^{[3]}\left[1-\pi^{H^2_{\sigma,\underline{\boldsymbol{\Psi}}_j}(x_{i:n}+1)}-c_{(i,n)}^{[2]}\right]\varpi_{(\underline{\boldsymbol{\Psi}}_j)}(x_{i:n}+1,\pi,\sigma,\underline{\boldsymbol{\Psi}}_j),$$

where $\varpi_{(\pi)}(x_{i:n}+1,\pi,\sigma,\underline{\boldsymbol{\Psi}}_j)$, $\varpi_{(\sigma)}(x_{i:n}+1,\pi,\sigma,\underline{\boldsymbol{\Psi}}_j)$ and $\varpi_{(\underline{\boldsymbol{\Psi}}_j)}(x_{i:n}+1,\pi,\sigma,\underline{\boldsymbol{\Psi}}_j)$ defined above.

4.2 Bayesian estimation

Before discussing how a Bayesian could estimate a population parameter, it is crucial to understand one key difference between frequentist and Bayesian statisticians. The difference is whether a statistician considers a parameter to be an unknowable constant or a random variable. An estimator or decision rule used in estimating theory and decision theory that minimizes the posterior expected value of a loss function is referred to as a Bayes estimator, also known as a Bayes action (i.e., the posterior expected loss). In other words, it maximizes the posterior expectation of the utility function. In the context of Bayesian statistics, maximum of a posteriori estimate is a distinct method of creating an estimator. Therefore, the numerical approximation is necessary. A set of algorithms known as Markov chain Monte Carlo (MCMC) techniques is used in statistics to sample probability distributions. By creating a Markov chain with the desired distribution as its equilibrium distribution and recording states from the chain, one may obtain a sample of the desired distribution. As the number of steps rises, the sample distribution closely mimics the actual target distribution. Several techniques are available for chain creation, most notably the Metropolis-Hastings algorithm.

Assume the beta, gamma and uniform priors for the parameters π,σ and $\underline{\boldsymbol{\Psi}}_j$ respectively. Then,

$$\mathcal{p}_{1,(\phi_1,\psi_1)}(\pi)\sim\text{beta}(\phi_1,\psi_1),$$
$$\mathcal{p}_{2,(\phi_2,\psi_2)}(\sigma)\sim\text{Gamma}(\phi_2,\psi_2),$$

and

$$\mathcal{p}_{3,(\phi_3,\psi_3)}(\underline{\boldsymbol{\Psi}}_j)\sim\text{Uniform}(\phi_3,\psi_3).$$

Assume that the parameters are independently distributed. The joint prior distribution $p_{(\phi_i,\psi_i)}(\pi,\sigma,\underline{\boldsymbol{\Psi}}_j)$ is given by

$$\mathcal{p}_{(\phi_i,\psi_i)}(\pi,\sigma,\underline{\boldsymbol{\Psi}}_j)=\frac{{\psi_2}^{\phi_1}}{(\psi_3-\phi_3)B(\phi_1,\psi_1)\Gamma(\phi_2)}\sigma^{\phi_1-1}exp(-\sigma\psi_2)\,\pi^{\phi_1}(1-\pi)^{\psi_1},$$

where $\mathrm{B}(\cdot,\cdot)$ is the beta function. The posterior distribution $p(\pi,\sigma,\underline{\boldsymbol{\Psi}}_j|\underline{z})$ of the parameters is defined as

$$\mathcal{p}(\pi,\sigma,\underline{\boldsymbol{\Psi}}_j|\underline{z})\propto\text{likelihood function}\times p_{(\phi_i,\psi_i)}(\pi,\sigma,\underline{\boldsymbol{\Psi}}_j).$$

Under SELF, the Bayesian estimators of $\pi,\ \sigma$ and $\underline{\boldsymbol{\Psi}}_j$ are the means of their marginal. It is not possible to obtain the Bayesian estimates through the above formulae. So, the numerical approximations are needed. We propose the use of MCMC techniques namely Gibbs sampler and M-H algorithm (see Cai (2010), Chib and Greenberg (1995) and Korkmaz et al. (2019) for more details). Since the conditional posteriors of the parameters $\pi,\ \sigma$ and $\underline{\boldsymbol{\Psi}}_j$ cannot be

obtained in any standard forms, using a hybrid MCMC for drawing sample from the marginal posterior of the parameters is suggested. Then, the full conditional posteriors of $\pi,\ \sigma$ and $\underline{\boldsymbol{\Psi}}_j$ can be easily derived. The simulation algorithm is given by:

1. Provide the initial values, say $\pi,\ \sigma$ and $\underline{\boldsymbol{\Psi}}_j$ then at i^{th} stage,
2. Using M-H algorithm, generate $\pi_{(i)} \sim \mathcal{P}_1\left(\pi_{(i)}|\pi_{(i-1)}, \sigma_{(i-1)}, \underline{\boldsymbol{\Psi}}_{j\,(i-1)}, \underline{x}\right)$,
3. Using M-H algorithm, generate $\sigma_{(i)} \sim \mathcal{P}_2\left(\sigma_{(i)}|\pi_{(i)}, \sigma_{(i-1)}, \underline{\boldsymbol{\Psi}}_{j\,(i-1)}, \underline{x}\right)$,
4. Using M-H algorithm, generate $\underline{\boldsymbol{\Psi}}_{j\,(i)} \sim \mathcal{P}_3\left(\underline{\boldsymbol{\Psi}}_{j\,(i)}|\pi_{(i)}\sigma_{(i)}, \underline{\boldsymbol{\Psi}}_{j\,(i-1)}, \underline{x}\right)$,

4.Repeat steps $1-4$, $M = 100000$ times to obtain the sample of size M from the corresponding posteriors of interest. Obtain the Bayesian estimates of $\pi,\ \sigma$ and $\underline{\boldsymbol{\Psi}}_j$ using the following formulae

$$\hat{\pi}_{\text{Bayesian}} = \frac{1}{M - M_0} \sum_{h=1+M_0}^{M} \pi^{[h]},$$

$$\hat{\sigma}_{\text{Bayesian}} = \frac{1}{M - M_0} \sum_{h=1+M_0}^{M} \sigma^{[h]},$$

and

$$\widehat{\underline{\boldsymbol{\Psi}}_j}_{\text{Bayesian}} = \frac{1}{M - M_0} \sum_{h=1+M_0}^{M} \underline{\boldsymbol{\Psi}}_j{}^{[h]},$$

respectively, where $M_0(\approx 50000)$ is the burn-in period of the generated MCMC.

5. Simulations for comparing non-Bayesian and Bayesian estimation methods

A MCMC simulation study is conducted for the DGR-W scenario in order to evaluate and contrast the performance of non-Bayesian and Bayesian estimates. The mean squared errors are used to accomplish the numerical assessment (MSEs). First, using n=50, 150, 300, and 500, we produced 1000 samples of the DGR-W distribution. In Table 1, Table 2, and Table 3, the MSEs are derived and listed. On the basis of Tables 1, 2, and 3, we may conclude that all approaches work well. Although in some circumstances the Bayesian approach is preferable. When n increases, all estimate techniques perform better and gravitate toward 0. The MLE method is still the most effective and consistent of the remaining classic methods, despite their diversity and abundance. However, most of the other classic methods are not as efficient or consistent as the MLE method, which is why it is generally noted that the MLE and the Bayesian methods are recommended for statistical modeling and applications. This assessment is shown in Table 1, Table 2 and Table 3. This Section uses simulation studies to assess various estimating approaches rather than to contrast them, however this does not exclude the use of simulation to contrast various estimation approaches. However, actual data is frequently used to evaluate various estimating techniques, which is why we will describe four examples especially for this function. To compare the rival models, there are further four more applications to count data.

Table 1: MSEs for π=0.55 , $\sigma = 0.9$ and θ=1.5

n		MLE	OLS	WLS	Bayesian
50	π	0.00540	0.00126	0.00183	0.00073
	σ	0.00701	0.02078	0.01465	0.00562
	θ	0.00696	0.00095	0.00120	0.00073
150	π	0.00141	0.00041	0.00070	0.00054
	σ	0.00169	0.00521	0.00197	0.00352
	θ	0.00169	0.00045	0.00045	0.00018
300	π	0.00062	0.00029	0.00048	0.00025
	σ	0.00078	0.00256	0.00154	0.00057
	θ	0.00078	0.00028	0.00023	0.00004

Table 2: MSEs for π=0.4 , σ=1.2 and θ=1.2

n		MLE	OLS	WLS	Bayesian
50	π	0.00429	0.00582	0.00523	0.00621
	σ	0.00686	0.03452	0.03015	0.00645
	θ	0.00683	0.01254	0.01245	0.02587
150	π	0.00142	0.00145	0.00153	0.00184
	σ	0.00226	0.00247	0.00185	0.00045
	θ	0.00226	0.00274	0.00295	0.00365
300	π	0.00065	0.00078	0.00078	0.00075
	σ	0.00103	0.00163	0.00084	0.00065
	θ	0.00103	0.00198	0.00193	0.00153

Table 3: MSEs for π=0.8 , σ=0.7 and θ=0.7

n		MLE	OLS	WLS	Bayesian
50	π	0.00105	0.00412	0.00326	0.02154
	σ	0.00426	0.00352	0.00287	0.00547
	θ	0.45841	0.00216	0.00356	0.00452
150	π	0.00032	0.00073	0.00205	0.00078
	σ	0.00135	0.00081	0.00045	0.00058
	θ	0.06960	0.00035	0.00088	0.00042
300	π	0.00016	0.00056	0.00145	0.00053
	σ	0.00070	0.00042	0.00025	0.00031
	θ	0.00536	0.00021	0.00064	0.00005

6. Real data modeling for comparing Bayesian and non-Bayesian methods

For the purpose of contrasting the Bayesian and non-Bayesian estimate approaches, four examples of real data sets are provided in this section. For comparing Bayesian and non-Bayesian estimating approaches, we take into account the Akaike information criterion (AIC) and Correct Akaike IC (CAIC) statistics.

6.1 Failure times data of 50 devices

According to Bebbington et al. (2012), this information indicates the failure rates of 50 devices submitted to a specific life test (in weeks). Table 4 lists the estimators for the AIC and CAIC statistics, Bayesian and non-Bayesian estimate techniques. Based on Table 4, the MLE method is the best method with Kolmogorov Smirnov (ks) test ks =0.1672 and p-value =0.1220, then the OLS method. However, the Bayesian and WLS methods do not perform well.

Table 4: Estimators under Bayesian and non-Bayesian estimation methods, AIC and CAIC statistics for 50 device failure rates' data.

Method	$\hat{\pi}$	$\hat{\theta}$	$\hat{\sigma}$	ks	p-value
MLE	**0.9923**	**0.2321**	**0.9777**	**0.1672**	**0.1220**
OLS	0.9898	0.2040	0.8908	0.2098	0.0245
WLS	0.9843	0.2792	2.2852	0.2209	0.0152
Bayesian	0.9255	0.1884	2.0864	0.2684	0.0015

6.2 Failure times of 15 electronic components

In an acceleration lifetime test, this lifetime data provides the failure durations for 15 electrical components (see Lawless (2003)). For the fifteen electrical components' failure rates data, Table 5 lists the estimators for the Bayesian and non-Bayesian estimating techniques, AIC and CAIC statistics. Based on Table 5, the WLS method is the best method with ks =0.0938 and p-value =0.9994, then the OLS method and then the MLE method. However, the Bayesian method does not perform well.

Table 5: Estimators under Bayesian and non-Bayesian estimation methods, AIC and CAIC statistics for the fifteen electrical components' failure rates data.

Method	$\hat{\pi}$	$\hat{\theta}$	$\hat{\sigma}$	ks	p-value
MLE	0.8289	0.2417	3.4122	0.1222	0.9785
OLS	0.9873	0.2288	0.9260	0.1029	0.9973
WLS	**0.9224**	**0.2228**	**2.0254**	**0.0938**	**0.9994**
Bayesian	0.8812	0.2146	2.0003	0.2175	0.4771

6.3 Counts of cysts of kidneys

This information shows the numbers of cysts in kidney dysmorphogenetic caused by corticosteroids and linked to uncontrolled production of Indian hedgehog and other recognized cytogenic molecules (see Chan et al., 2009). Table 6 gives the estimators under Bayesian and non-Bayesian estimation methods, AIC and CAIC statistics for numbers of kidney cysts. Based on Table 6, the MLE method is the best method with ks =0.7660 and p-value =0.6818, then the Bayesian method then the WLS method. However, the OLS method does not perform well.

Table 6: Estimators under Bayesian and non-Bayesian estimation methods, AIC and CAIC statistics for numbers of kidney cysts.

Method	$\hat{\pi}$	$\hat{\theta}$	$\hat{\sigma}$	ks	p-value
MLE	**0.6791**	**0.1799**	**1.1202**	**0.7660**	**0.6818**
OLS	0.8020	0.1539	0.8233	3.4632	0.1770
WLS	0.9903	0.1901	0.2036	2.3787	0.3044
Bayesian	0.6765	0.1729	1.1096	0.7048	0.7030

6.4 Number of European corn-borer larvae parasites

According to Bodhisuwan and Sangpoom (2016), this information reflects the quantity of parasitic European corn-borer larvae in the field. Bodhisuwan and Sangpoom (2016) randomly chose 8 hills from 15 replications for their stochastic biological experiment and counted the number of corn borers on each hill. Table 7 gives the estimators under Bayesian and non-Bayesian estimation methods, AIC and CAIC statistics for **number of European corn-borer larvae parasites data**. Based on Table 7, the MLE method is the best method with ks =0.8160 and p-value =0.6650, then the Bayesian method. However, the OLS and the WLS method does not perform well.

Table 7: Estimators under Bayesian and non-Bayesian estimation methods, AIC and CAIC statistics for **number of European corn-borer larvae parasites data**.

Method	$\hat{\pi}$	$\hat{\theta}$	$\hat{\sigma}$	ks	p-value
MLE	**0.0027**	**0.2218**	**3.3132**	**0.8160**	**0.6650**
OLS	0.2756	0.2194	1.8667	11.1726	0.0038
WLS	0.0877	0.2062	2.2879	11.4121	0.0033
Bayesian	0.2444	0.2150	2.1242	5.8520	0.0540

7. Real data modeling for comparing the competitive models

We illustrate the flexibility and the importance of the DGR-W distributions using four real data applications. The fitted distributions (see Table 8) are analyzed and compared using the log-likelihood function (ℓ), AIC, CAIC, Chi-square (χ^2_V) with degree of freedom (d.f) and its p-value, Kolmogorov-Smirnov ($K-S$) and its p-value. Table 4 below gives the competitive models.

7.1 Failure times data of 50 devices

We compare the DGR-W model's fits to those of other rival models, including DW, EDW, DIW, EDLi, DPa, DLi-II, and DLL. The goodness of fit (GOF) test statistics and the MLEs, together with their accompanying standard errors (SEs), are provided in Tables 9 and 10, respectively. For the analysis of data with a regularly distributed distribution, statisticians have created a potent collection of tools. The "normal quantile-quantile (Q-Q) plot" is the most well-liked one. All the quantile points would fall between the two blue lines if the data distribution precisely matched the normal distribution. The Q-Q plot is shown in Figure 3 (left plot) for 50 device failure rates' data. Figure 3 (right panel)

displays a box with statistics on failure rates (50 device failure rates' data). The HRF's form can influence which model is used for an application. The total time on test (TTT) plot is used for this purpose. It has a "convex form" for "monotonically dropping HRF" and a "concave shape" for "monotonically increasing HRF." When the solid line and dashed line coincide, the HRF of the data is said to be "continuous." For the DGR-W model for 50 device failure rates' data, Figure 4 displays the TTT plot (left panel) and estimated HRF (EHRF). The DGR-W offers the finest fits versus all competing models, according to Table 10.

Table 8: The competitive models.

	Discrete Model	Abbreviation
1	Pareto	DPa
2	Lomax	DLx
3	Lindley	DLi
4	Weibull	DW
5	Rayleigh	DR
6	Log-logistic	DLL
7	Exponential	DE
8	Burr type XII	DBXII
9	Lindley type II	DLi-II
10	Inverse Rayleigh	DIR
11	Poisson (Poisson (1837))	Poisson
12	Inverse Weibull	DIW
13	Exponentiated Weibull	EDW
14	Exponentiated Lindley	EDLi
15	Generalized Exponentiated type II	DGE-II
16	Negative Binomial (Dougherty (1992))	NB

Table 9: MLEs (SEs) for 50 device failure rates' data.

Model	$\hat{\pi}$	$\hat{\theta}$	$\hat{\sigma}$
DGR-W	**0.9923**	**0.2321**	**0.9777**
	(0.01106)	**(0.01779)**	**(0.67611)**
EDW	0.989	1.139	0.784
	(0.164)	(3.227)	(3.053)
DW	0.981	1.023	
	(0.011)	(0.131)	
DIW	0.018	0.582	
	(0.013)	(0.061)	
DLi-II	0.969	0.058	
	(0.005)	(0.027)	
EDLi	0.972	0.480	
	(0.005)	(0.087)	
DLLc	1.000	0.439	
	(0.321)	(0.062)	
DPa	0.739		
	(0.032)		

Table 10: The GOF statistics for 50 device failure rates' data.

Model↓	-ℓ	AIC	CAIC	K-S	p-value
DGR-W	**237.5**	**480.9**	**481.5**	**0.167**	**0.122**
EDW	240.2	486.7	487.2	0.195	0.045
DW	241.6	487.2	487.5	0.187	0.061
DIW	261.9	527.8	528.1	0.258	0.003
DLi-II	240.6	485.2	485.4	0.186	0.064
EDLi	240.3	484.6	484.8	0.195	0.045
DLLc	294.9	593.8	594.0	0.535	< 0.001
DPa	275.9	553.7	553.8	0.335	< 0.001

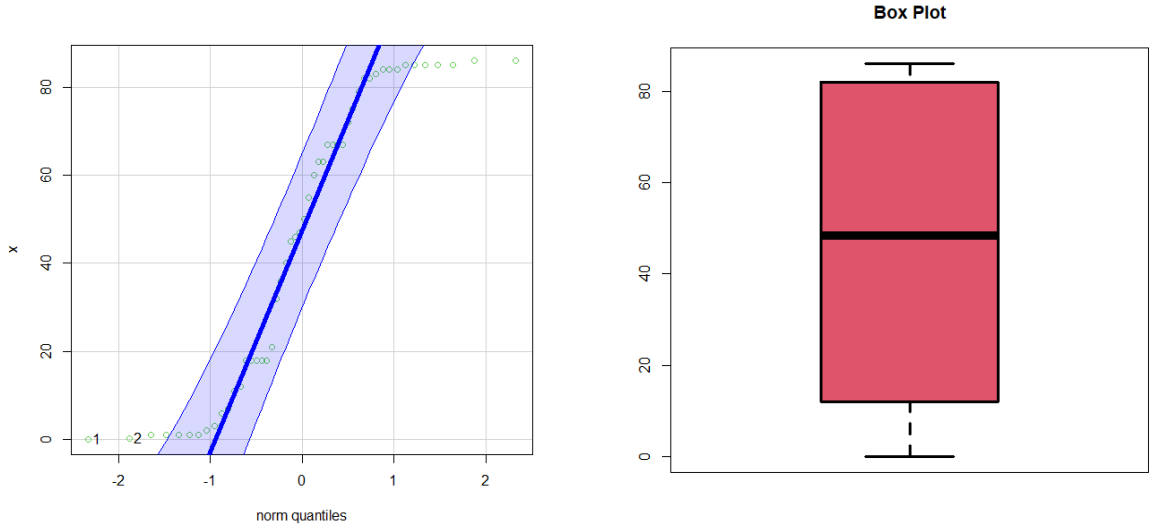

Figure 3: Q-Q plot and box for the failure times data.

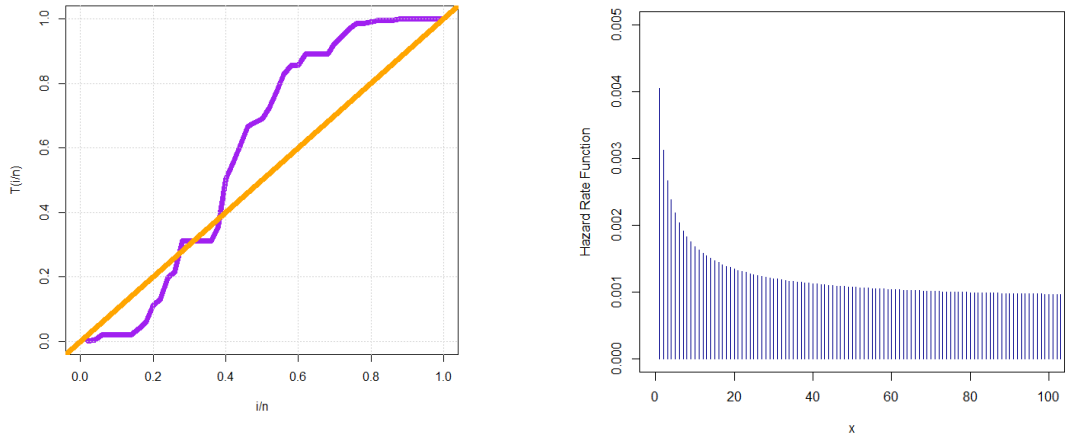

Figure 4: TTT plot and EHRF for the DGR-W model for 50 device failure rates' data.

7.2 Failure times of 15 electronic components

We compare the DGR-W model's fits to those of other rival models for this application, including DGE-II, DLx, DEx, DIR, DR, DIW, DPa, and DBXII. Tables 11 and 12, respectively, include information on the MLEs with their SEs and the GOF data. The Q-Q plot and box for the failure times data are shown in Figure 5. Figure 6 displays the estimated HRF (EHRF) and total time test plots (TTT) plots for the DGR-W model for the fifteen electrical components' failure rates data. The DGR-W offers the finest fits versus all competing models, according to Table 12.

Table 11: MLEs (SEs) for fifteen electrical components' failure rates.

Model	$\hat{\pi}$	$\hat{\theta}$	$\hat{\sigma}$
DGR-W	**0.8289**	**0.2417**	**3.4122**
	(0.8065)	**(0.0681)**	**(5.5934)**
DGE-II	0.9563	1.491	
	(0.0133)	(0.535)	
DIW	2.2×10^{-4}	0.875	
	(7.8×10^{-4})	(0.164)	
DLx	0.01243	104.506	
	(0.039)	(84.409)	
DBXII	0.9753	13.367	
	(0.051)	(27.785)	
DR	0.9991		
	(2.58×10^{-4})		
DIR	1.8×10^{-7}		
	(0.055)		
DPa	0.7202		
	(0.061)		
DE	0.9654		
	(0.0091)		

Table 12: The GOF statistics for fifteen electrical components' failure rates.

Model↓	-ℓ	AIC	CAIC	K-S	p-value
DGR-W	**63.9**	**133.9**	**136.1**	**0.122**	**0.978**
DE	65.0	134.0	136.3	0.177	0.673
DGE-II	64.4	134.8	135.8	0.129	0.937
DR	66.4	134.8	136.1	0.216	0.433
DIR	89.1	180.2	180.5	0.698	< 0.0001
DIW	68.7	141.4	142.4	0.209	0.482
DLx	65.9	135.7	136.7	0.205	0.491
DB-XII	75.7	155.5	156.5	0.388	0.015
DPa	77.4	156.8	157.1	0.405	0.009

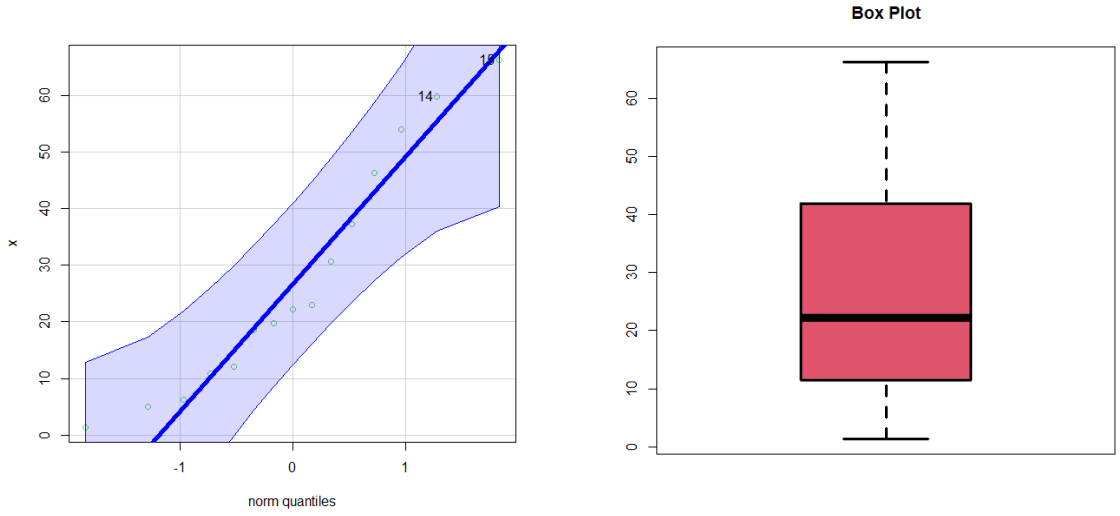

Figure 5: Q-Q plot and box for the failure times data (fifteen electrical components' failure rates).

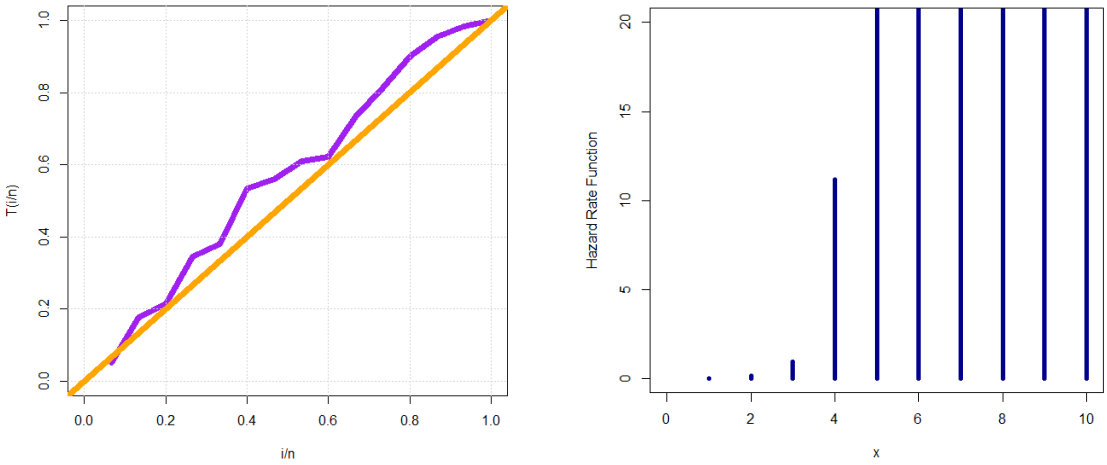

Figure 6: TTT plot and EHRF for the DGR-W model for fifteen electrical components' failure rates.

7.3 Counts of cysts of kidneys

We compare the DGR-W distribution's fits to those of the DW, DR, DIW, DE, DLx, DLi-II, DLi, and Poisson for this real data set. Table 13 includes a list of the MLEs together with their SEs. The GOF data are shown in Table 14. For numbers of kidney cysts, Figure 7 displays the TTT plot, Q-Q plot, and Box plot vs the EHRFs. The fitted PMFs and EHRF for numbers of kidney cysts are shown in Figure 8. The DGR-W offers the finest fits versus all competing models, according to Table 14.

Table 13: MLEs (SEs) for numbers of kidney cysts.

Model	$\hat{\pi}$	$\hat{\theta}$	$\hat{\sigma}$
DGR-W	**0.6761**	**0.1799**	**1.1202**
	(0.4551)	**(0.0269)**	**(0.7666)**
DW	0.750	0.431	
	(0.084)	(0.340)	
DIW	0.581	1.049	
	(0.048)	(0.146)	
DLi-II	0.581	0.001	
	(0.045)	(0.058)	
DLx	0.150	1.830	
	(0.098)	(0.951)	
DR	0.901		
	(0.009)		
DE	0.581		
	(0.030)		
DLi	0.436		
	(0.026)		
Poisson	1.390		
	(0.112)		

Table 14: The GOF statistics for fifteen electrical components' failure ratesI.

Z	OF	**DGR-W**	DW	DIW	DR	DEx	DLi	DLi-II	DLx	Poisson
0	65	**63.4**	59.01	63.91	11.00	46.09	40.25	46.03	61.89	27.42
1	14	**16.65**	19.84	20.70	26.83	26.78	29.83	26.77	21.01	38.08
2	10	**9.37**	10.78	8.05	29.55	15.56	18.36	15.57	9.65	26.47
3	6	**5.95**	6.26	4.23	22.23	9.04	10.35	9.05	5.24	12.26
4	4	**4.00**	4.19	2.60	12.49	5.25	5.53	5.27	3.17	4.26
5	2	**2.79**	2.01	1.75	5.42	3.05	2.86	3.06	2.06	1.18
6	2	**1.99**	1.99	1.26	1.85	1.77	1.44	1.78	1.42	0.27
7	2	**1.45**	1.32	0.95	0.52	1.03	0.71	1.04	1.02	0.05
8	1	**1.07**	0.99	0.74	0.11	0.60	0.35	0.60	0.76	0.01
9	1	**0.80**	0.86	0.59	0.02	0.35	0.17	0.35	0.58	0.00
10	1	**0.60**	0.76	0.48	0.00	0.20	0.08	0.20	0.46	0.00
11	2	**0.46**	1.99	4.74	0.00	0.28	0.07	0.28	2.74	0.00
-ℓ		**167.48**	170.14	172.93	277.78	178.77	189.1	178.8	170.48	246.21
AIC		**340.96**	344.28	349.87	557.56	359.53	380.2	361.5	344.96	494.42
CAIC		**341.19**	344.39	349.98	557.59	359.57	380.3	361.6	345.07	494.46
χ^2		**0.766**	3.125	6.463	321.07	22.88	43.48	22.89	3.316	294.10
d.f		**2**	3	3	4	4	4	3	3	4
p-value		**0.682**	0.373	0.091	<0.0001	0.0001	<0.0001	<0.0001	0.345	<0.0001

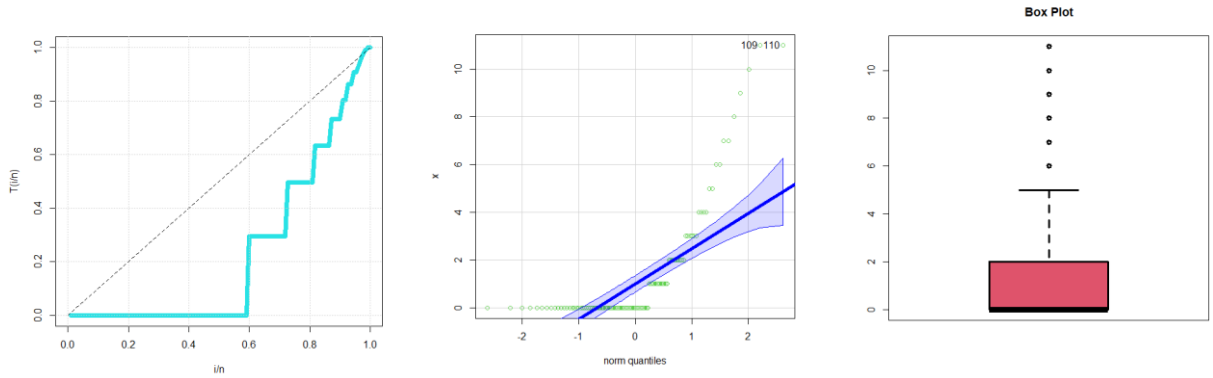

Figure 7: TTT plot, Q-Q plot and Box plot versus the EHRFs for numbers of kidney cysts.

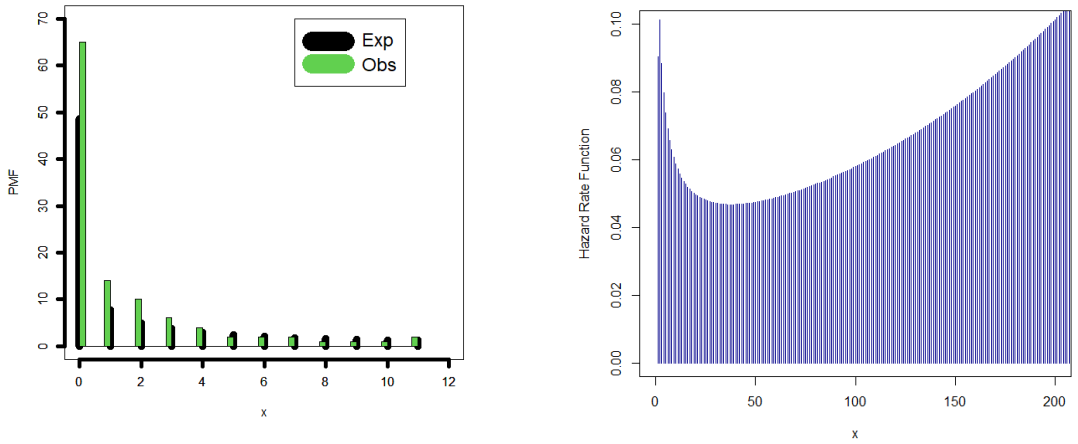

Figure 8: The fitted PMFs and EHRF for numbers of kidney cysts.

7.4 Number of European corn-borer larvae parasites

We will evaluate how well DIW, DGIW, DIR, DPa, DR, DBXII, NB, and Poisson distributions match the DGR-W distributions. Table 15 gives the MLEs together with the matching SEs. The GOF data are shown in Table 16. For the number of European corn-borer larvae parasites, Figure 9 displays the TTT plot, Q-Q plot, and box plot vs the EHRFs. The fitted PMFs and EHRF for number of European corn-borer larvae parasites are shown in Figure 10. The DGR-W offers the finest fits versus all competing models, according to Table 16.

Table 15: MLEs (SEs) for number of European corn-borer larvae parasites.

Model	$\hat{\pi}$	$\hat{\theta}$	$\hat{\sigma}$	$\hat{\beta}$
DGR-W	**0.0027**	**0.2218**	3.3132	
	(0.0096)	**(0.0225)**	(0.5337)	
DGW	0.0450	2.539	2.159	0.479
	(0.429)	(4.703)	(2.698)	(0.466)
DIW	0.3454	1.5414		
	(0.043)	(0.156)		
DBXII	0.5193	2.358		
	(0.051)	(0.366)		
NB	0.8703	9.956		
	(0.036)	(0.096)		
DIR	0.319			
	(0.042)			
DR	0.867			
	(0.012)			
DPa	0.3293			
	(0.034)			
Poisson	1.4836			
	(0.025)			

Table 16: The GOF statistics for number of European corn-borer larvae parasites.

Z	OF	**DGR-W**	DIW	DBXII	DIR	DR	NB	DPa	Poisson
0	43	**44.57**	41.37	43.84	38.28	15.92	30.12	64.45	27.23
1	35	**30.86**	41.85	39.61	51.90	36.17	38.87	20.15	40.38
2	17	**18.94**	15.42	15.62	15.51	34.58	27.61	9.69	29.95
3	11	**11.20**	7.17	7.20	6.04	21.03	14.26	5.65	14.81
4	5	**6.45**	3.94	3.91	2.91	8.89	5.99	3.68	
5	4	**3.64**	2.42	2.37	1.61	2.70	2.17	2.58	1.63
6	1	**2.01**	1.61	1.56	0.98	0.60	0.70	1.90	0.40
7	2	**1.1**	1.13	1.09	0.64	0.09	0.21	1.46	0.09
8	2	**0.59**	5.09	4.80	2.14	0.02	0.06	10.44	0.02
-ℓ		**200.31**	204.810	204.293	208.440	235.23	211.52	220.63	219.19
AIC		**406.61**	413.621	412.587	418.881	472.45	427.05	443.24	440.38
CAIC		**406.82**	413.723	412.689	418.915	472.49	427.14	443.27	440.41
χ^2		**0.816**	5.511	4.664	14.274	70.688	20.367	32.462	38.478
d.f		**2**	3	3	4	4	3	4	4
p-value		**0.665**	0.138	0.198	< 0.0001	< 0.0001	0.0001	< 0.0001	< 0.0001

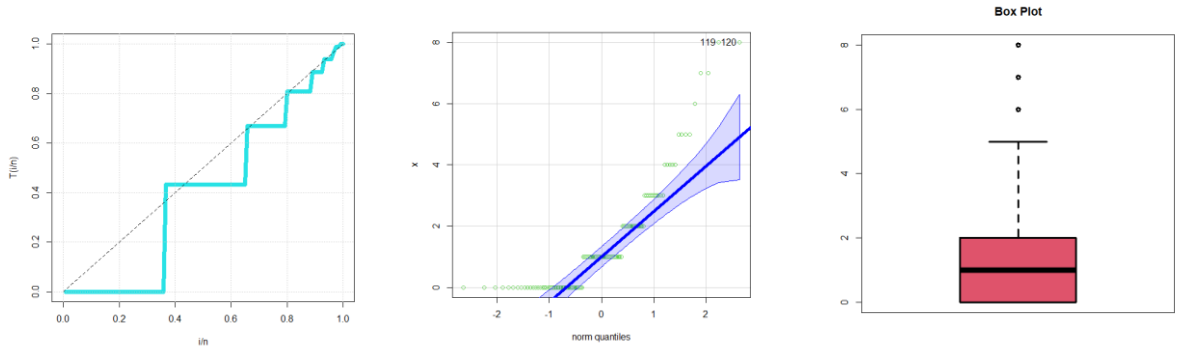

Figure 9: TTT plot, Q-Q plot and box plot versus the EHRFs for data set number of European corn-borer larvae parasites.

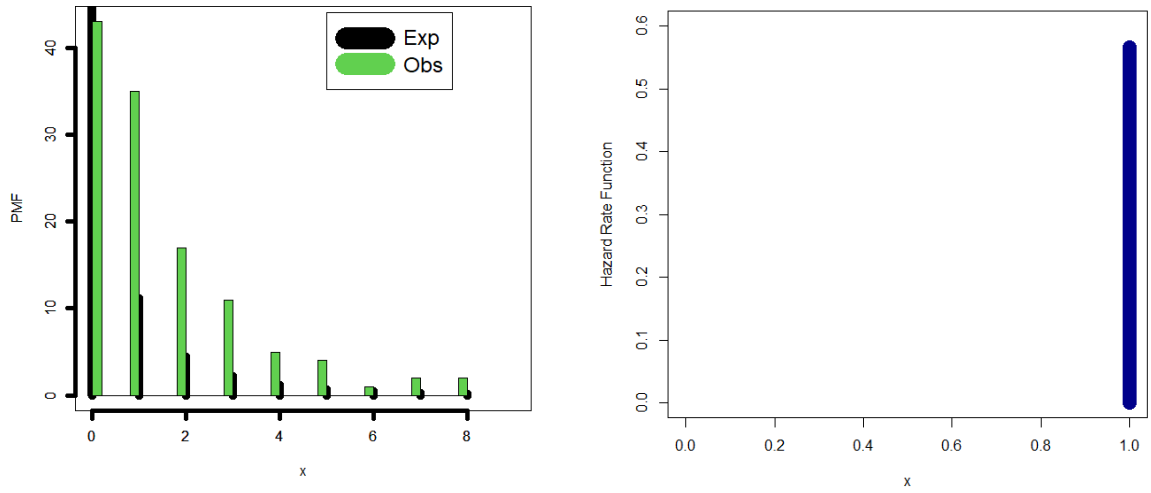

Figure 10: The fitted PMFs and EHRF for data set number of European corn-borer larvae parasites.

8. Concluding remarks

In this study, we introduced and investigated the discrete generated Rayleigh G (DGR-G) family of distributions, a novel discrete counterpart based on the continuous Rayleigh distribution. Moments, cumulant generating function, L-moments, moment generating function, probability generating function, central moment, and dispersion index are some of its statistical features that are derived. It is described how a Weibull distribution relates to a specific discrete variant of the DGR-G family.

A particular case is investigated and visually examined. The new hazard rate function offers a broad range of flexibilities, including "monotonically decreasing," "upside down", "monotonically increasing", "constant," "decreasing-constant" and "decreasing-constant-increasing (U- hazard rate function)". Moreover, the new probability mass function accommodates many useful forms in the field of modeling, including the "right skewed with one peak", "right skewed with two peaks (right skewed and bimodal)", "symmetric mass function", "left skewed with one peak". Some pertinent characterizations results are generated and provided using the conditional expectation of a certain function of the random variable of the hazard function. Also, the Bayesian process under the SELF is shown in detail, it is advised to take samples from the joint posterior of the parameters as the conditional posteriors of the parameters cannot be obtained in any conventional forms. To compare non-Bayesian versus Bayesian estimates, MCMC simulations are run. Gibbs sampling and the M-H method are used. The Bayesian approach offers the lowest mean

squared errors across all sample sizes. The non-Bayesian estimating techniques work admirably but fall short of the Bayesian approach, the performance for all estimation methods (Bayesian and non-Bayesian) improves as n increases.

The Bayesian and non-Bayesian approaches are compared using four real-world applications of data sets. Four real data applications are used to highlight the new discrete class's significance and adaptability. Various unique member distributions might be considered and researched in separate studies in the future. Future research may consider the DGR-G family's bivariate and multivariate expansions. We anticipate that the DGR-G family will draw more applications in engineering, dependability, and other fields of study. Particularly in terms of the statistical testing of hypotheses and validation, whether in the case of complete data or in the case of censored data, discrete distributions still require more research and applications.

The DGR-G family offered a powerful and flexible framework for modeling count data in reliability engineering and related fields. It stands out due to its ability to capture a wide range of hazard rate shapes, such as monotonically decreasing, increasing, constant, bathtub-shaped, and more complex forms like decreasing-constant-increasing. This versatility made it especially valuable for modeling failure times and events counts where the risk of occurrence evolves over time in non-trivial ways. Unlike many traditional discrete distributions, the DGR-G family can accommodate zero-inflation, over-dispersion, and multimodal structures commonly seen in real-world datasets. Its probability mass function exhibits diverse shapes, including right-skewed, left-skewed, symmetric, and bimodal forms, enhancing its applicability across various domains. The model was rigorously evaluated using both classical and Bayesian estimation techniques, showing superior performance in terms of accuracy and robustness, particularly in small sample sizes. When applied to real-world data from engineering, medical, and agricultural contexts, the DGR-G family consistently outperformed 16 existing discrete models in goodness-of-fit measures. These applications included failure times of electronic components, counts of kidney cysts, and parasitic insect populations, demonstrating the model's adaptability to different types of count data. The theoretical characterizations based on truncated moments and hazard function properties further support its statistical foundation. With potential extensions into multivariate settings and regression modeling, the DGR-G family represents a promising tool for future research and practical use in reliability analysis and beyond.

Contributions: All authors participated equally in the preparation of the paper and have equal shares in all types of contributions.

Data Availability: Data will be provided by Haitham M. Yousof upon request.

Conflict of interests: The authors declare that there is no conflict of interests.

Acknowledgments: This work was supported by the Deanship of Scientific Research, Vice Presidency for Graduate Studies and Scientific Research, King Faisal University, Saudi Arabia [Grant No. KFU252917].

References

1. Aboraya, M., M. Yousof, H. M., Hamedani, G. G., & Ibrahim, M. (2020). A new family of discrete distributions with mathematical properties, characterizations, Bayesian and non-Bayesian estimation methods. Mathematics, 8, 1648.
2. Bebbington, M., Lai, C. D., Wellington, M., & Zitikis, R. (2012). The discrete additive Weibull distribution: A bathtub-shaped hazard for discontinuous failure data. Reliability Engineering & System Safety, 106, 37-44.
3. Bodhisuwan, W., & Sangpoom, S. (2016, October). The discrete weighted Lindley distribution. In 2016 12th International Conference on Mathematics, Statistics, and Their Applications (ICMSA) (pp. 99-103). IEEE.
4. Cai, L. (2010). Metropolis-Hastings Robbins-Monro algorithm for confirmatory item factor analysis. Journal of Educational and Behavioral Statistics, 35(3), 307-335.
5. Chib, S., & Greenberg, E. (1995). Understanding the metropolis-hastings algorithm. The american statistician, 49(4), 327-335.
6. Consul, P. C., & Jain, G. C. (1973). A generalization of the Poisson distribution. Technometrics, 15(4), 791-799.
7. Chan, S. K., Riley, P. R., Price, K. L., McElduff, F., Winyard, P. J., Welham, S. J., ... & Long, D. A. (2010). Corticosteroid-induced kidney dysmorphogenesis is associated with deregulated expression of known cystogenic molecules, as well as Indian hedgehog. American journal of physiology-renal physiology, 298(2), F346-F356.

8. Chesneau, C., Yousof, H., Hamedani, G. G., & Ibrahim, M. (2022). The Discrete Inverse Burr Distribution with Characterizations, Properties, Applications, Bayesian and Non-Bayesian Estimations. Statistics, Optimization & Information Computing, 10(2), 352-371.
9. Cordeiro, G. M., Yousof, H. M., Ramires, T. G., & Ortega, E. M. (2018). The Burr XII system of densities: properties, regression model and applications. Journal of Statistical Computation and Simulation, 88(3), 432-456.
10. Dougherty, E. R. (1990). Probability and statistics for the engineering, computing, and physical sciences. Prentice-Hall, Inc.
11. Eliwa, M. S., Alhussain, Z. A., & El-Morshedy, M. (2020). Discrete Gompertz-G family of distributions for over-and under-dispersed data with properties, estimation, and applications. Mathematics, 8(3), 358.
12. Eliwa, M. S., El-Morshedy, M., Yousof, H. M. (2022). A Discrete Exponential Generalized-G Family of Distributions: Properties with Bayesian and Non-Bayesian Estimators to Model Medical, Engineering and Agriculture Data. Mathematics, 10, 3348. https://doi.org/10.3390/math10183348
13. El-Morshedy, M., Eliwa, M. S., & Altun, E. (2020). Discrete Burr-Hatke distribution with properties, estimation methods and regression model. IEEE access, 8, 74359-74370.
14. El-Morshedy, M., Eliwa, M. S., & Tyagi, A. (2022). A discrete analogue of odd Weibull-G family of distributions: properties, classical and Bayesian estimation with applications to count data. Journal of Applied Statistics, 49(11), 2928-2952.
15. El-Morshedy, M., Eliwa, M. S., & Nagy, H. (2020). A new two-parameter exponentiated discrete Lindley distribution: properties, estimation and applications. Journal of applied statistics, 47(2), 354-375.
16. Gómez-Déniz, E. (2010). Another generalization of the geometric distribution. Test, 19(2), 399-415.
17. Gómez-Déniz, E., & Calderín-Ojeda, E. (2011). The discrete Lindley distribution: properties and applications. Journal of statistical computation and simulation, 81(11), 1405-1416.
18. Hamedani, G. G., Yousof, H. M., Rasekhi, M., Alizadeh, M., & Najibi, S. M. (2018a). Type I general exponential class of distributions. Pakistan Journal of Statistics and Operation Research, 39-55.
19. Hamedani, G. G., Altun, E., Mustafa, Ã., Yousof, H. M., & Butt, N. S. (2018b). A new extended G family of continuous distributions with mathematical properties, characterizations and regression modeling. Pakistan Journal of Statistics and Operation Research, 737-758.
20. Hamedani, G. G., Rasekhi, M., Najibi, S., Yousof, H. M., & Alizadeh, M. (2019). Type II general exponential class of distributions. Pakistan Journal of Statistics and Operation Research, 503-523.
21. Hussain, T., & Ahmad, M. (2014). DISCRETE INVERSE RAYLEIGH DISTRIBUTION. Pakistan Journal of Statistics, 30(2).
22. Hussain, T., Aslam, M., & Ahmad, M. (2016). A two parameter discrete Lindley distribution. Revista Colombiana de EstadÝstica, 39(1), 45-61.
23. Ibrahim, M., Ali, M. M. and Yousof, H. M. (2021). The discrete analogue of the Weibull G family: properties, different applications, Bayesian and non-Bayesian estimation methods. Annals of Data Science, https://link.springer.com/article/10.1007/s40745-021-00327-y
24. Jazi, M. A., Lai, C. D., & Alamatsaz, M. H. (2010). A discrete inverse Weibull distribution and estimation of its parameters. Statistical Methodology, 7(2), 121-132.
25. Kemp, A. W. (2004). Classes of discrete lifetime distributions. Commun. Stat. Theor. Methods. 2004, 33(12), 3069--3093.
26. Kemp, A. W. (2008). The discrete half-normal distribution. In Advances in mathematical and statistical modeling (pp. 353-360). Birkhäuser Boston.
27. Korkmaz, M. Ç., Altun, E., Yousof, H. M., & Hamedani, G. G. (2019). The odd power Lindley generator of probability distributions: properties, characterizations and regression modeling. International Journal of Statistics and Probability.
28. Korkmaz, M. Ç., Yousof, H. M., Hamedani, G. G., & Ali, M. M. (2018a). Pak. J. Statist. 2018 Vol. 34 (3), 251-267 The Marshall-Olkin generalized G Poisson family of distributions. Pak. J. Statist, 34(3), 251-267.
29. Korkmaz, M. C., Yousof, H. M., Rasekhi, M., & Hamedani, G. G. (2018b). The odd Lindley Burr XII model: Bayesian analysis, classical inference and characterizations. Journal of data science, 16(2), 327-353.
30. Krishna, H., & Pundir, P. S. (2009). Discrete Burr and discrete Pareto distributions. Statistical methodology, 6(2), 177-188.
31. Lawless, J. F. (2011). Statistical models and methods for lifetime data. John Wiley & Sons.
32. Nakagawa, T., & Osaki, S. (1975). The discrete Weibull distribution. IEEE transactions on reliability, 24(5), 300-301.
33. Nekoukhou, V., & Bidram, H. (2015). The exponentiated discrete Weibull distribution. Sort, 39, 127-146.

34. Nekoukhou, V., Alamatsaz, M. H., & Bidram, H. (2013). Discrete generalized exponential distribution of a second type. Statistics, 47(4), 876-887.
35. Nascimento, A. D., Silva, K. F., Cordeiro, G. M., Alizadeh, M., Yousof, H. M., & Hamedani, G. G. (2019). The odd Nadarajah-Haghighi family of distributions: properties and applications. Studia Scientiarum Mathematicarum Hungarica, 56(2), 185-210.
36. Para, B. A., & Jan, T. R. (2016). Discrete version of log-logistic distribution and its applications in genetics. International Journal of Modern Mathematical Sciences, 14(4), 407-422.
37. Para, B. A., & Jan, T. R. (2016). On discrete three-parameter Burr type XII and discrete Lomax distributions and their applications to model count data from medical science. Biometrics and Biostatistics International Journal, 4(2), 1-15.
38. Poisson, S. D. (1837). Recherches sur la probabilité des jugements en matière criminelle et en matière civile: précédées des règles générales du calcul des probabilités. Bachelier.
39. Roy, D. (2004). Discrete rayleigh distribution. IEEE Transactions on Reliability, 53(2), 255-260.
40. Yousof, H. M., Chesneau, C., Hamedani, G. and Ibrahim, M. (2021). A New Discrete Distribution: Properties, Characterizations, Modeling Real Count Data, Bayesian and Non-Bayesian Estimations. Statistica, 81(2), 135-162.